State of the Global Climate 2022

WEATHER CLIMATE WATER

WORLD METEOROLOGICAL ORGANIZATION

WMO-No. 1316

We need your feedback

This year, the WMO team has launched a process to gather feedback on the State of the Climate reports and areas for improvement. Once you have finished reading the publication, we ask that you kindly give us your feedback by responding to this short survey. Your input is highly appreciated.

WMO-No. 1316

Chair, Publications Board
World Meteorological Organization (WMO)
7 bis, avenue de la Paix
P.O. Box 2300
CH-1211 Geneva 2, Switzerland

Tel.: +41 (0) 22 730 84 03
Fax: +41 (0) 22 730 81 17
Email: publications@wmo.int

ISBN 978-92-63-11316-0

Cover illustration from Adobe Stock: Lightning storm over city in purple light (Photo credits: stnazkul, 84059942); Healthy Corals and Beautiful Islands in Wayag, Raja Ampat (Photo credits: ead72, 134052652); Forest fire (Photo credits: Kirk Atkinson, 180656803); Drought cracked landscape, dead land due to water shortage (Photo credits: AA+W, 537083081); Antarctica beautiful landscape, blue icebergs, nature wilderness (Photo credits: Song_about_summer, 217568993); Haboob dust storm in the Arizona desert (Photo credits: JSirlin, 256749173); Hurricane from space. The atmospheric cyclone. Elements of this image furnished by NASA (Photo credits: Viks_jin, 529897598)

Contents

Key messages . . . . . **ii**

Foreword . . . . . **iii**

Global climate indicators **1**

Baselines 1

Greenhouse gases 1

Temperature 3

Ocean 4

Cryosphere 12

Stratospheric ozone and ozone-depleting gases 19

Precipitation 20

Short-term climate drivers 21

Extreme events **24**

Heat, drought and wildfires 24

Cold extremes 27

Flooding and heavy rain 28

Tropical cyclones 29

Severe storms 31

Socioeconomic impacts **32**

Food security 32

Population displacement 34

Climate impacts on ecosystems and the environment 36

Updating the climatological normal to 1991–2020 . . . . . ***38***

Observational basis for climate monitoring ***40***

Data sets and methods **42**

List of contributors **48**

Key messages

The global mean temperature in 2022 was 1.15 [1.02–1.28] °C above the 1850–1900 average. The years 2015 to 2022 were the eight warmest in the 173-year instrumental record. The year 2022 was the fifth or sixth warmest year on record, despite ongoing La Niña conditions.

The year 2022 marked the third consecutive year of La Niña conditions, a duration which has only occurred three times in the past 50 years.

Concentrations of the three main greenhouse gases – carbon dioxide, methane and nitrous oxide – reached record highs in 2021, the latest year for which consolidated global values are available (1984–2021). The annual increase in methane concentration from 2020 to 2021 was the highest on record. Real-time data from specific locations show that levels of the three greenhouse gases continued to increase in 2022.

Around 90% of the energy trapped in the climate system by greenhouse gases goes into the ocean. Ocean heat content, which measures this gain in energy, reached a new observed record high in 2022.

Despite continuing La Niña conditions, 58% of the ocean surface experienced at least one marine heatwave during 2022. In contrast, only 25% of the ocean surface experienced a marine cold spell.

Global mean sea level continued to rise in 2022, reaching a new record high for the satellite altimeter record (1993–2022). The rate of global mean sea level rise has doubled between the first decade of the satellite record (1993–2002, 2.27 mm per year) and the last (2013–2022, 4.62 mm per year).

In the hydrological year 2021/2022, a set of reference glaciers with long-term observations experienced an average mass balance of –1.18 m water equivalent (m w.e.). This loss is much larger than the average over the last decade. Six of the ten most negative mass balance years on record (1950–2022) occurred since 2015. The cumulative mass balance since 1970 amounts to more than –26 m w.e.

In East Africa, rainfall has been below average in five consecutive wet seasons, the longest such sequence in 40 years. As of August 2022, an estimated 37 million people faced acute food insecurity across the region, under the effects of the drought and other shocks.

Record-breaking rain in July and August led to extensive flooding in Pakistan. There were at least 1 700 deaths, and 33 million people were affected, while almost 8 million people were displaced. Total damage and economic losses were assessed at US$ 30 billion.

Record-breaking heatwaves affected China and Europe during the summer. In some areas, extreme heat was coupled with exceptionally dry conditions. Excess deaths associated with the heat in Europe exceeded 15 000 in total across Spain, Germany, the United Kingdom, France and Portugal.

Foreword

This report shows that, once again, greenhouse gas concentrations in the atmosphere continue to reach record levels – contributing to warming of the land and ocean, melting of ice sheets and glaciers, rising sea levels, and warming and acidifying of oceans. There are major gaps in the weather and climate observing networks, especially in the least developed countries (LDCs) and small island developing States (SIDS), which is an obstacle for climate baseline monitoring, especially at regional and national scales, and for the provision of early warning and adequate climate services. WMO works with its members and partners to improve climate observations through the Global Climate Observing System (GCOS) and by ensuring adequate financial mechanisms for weather and climate observations through the Systematic Observations Financing Facility (SOFF).

While emissions continue to rise and the climate continues to change, vulnerable populations continue to be gravely impacted by extreme weather and climate events. For example, in 2022, continuing drought in East Africa, record-breaking rainfall in Pakistan and record-breaking heatwaves in China and Europe affected tens of millions, drove food insecurity, led to mass migration, and cost billions of dollars in loss and damage. However, collaboration amongst United Nations agencies has proven to be very effective in addressing humanitarian impacts induced by extreme weather and climate events, especially in reducing associated mortality and economic losses.

The United Nations Early Warnings for All Initiative, spearheaded by WMO, aims to fill the existing capacity gap to ensure that every person on Earth is covered by early warning services. Achieving this ambitious task requires sound observations and regular updates on key climate indicators, as provided in this report.

WMO is also preparing a new scheme for monitoring the sinks and sources of the main greenhouse gases based on modelling and on ground-based and satellite measurements. The scheme will enable better understanding of the uncertainties related to the strength of carbon sinks and sources associated with land use, as well as those related to the sources of methane.

I take this opportunity to congratulate and thank the experts and lead author, who jointly compiled this report using physical data analyses and impact assessments, and to thank all the contributors, particularly WMO Member National Meteorological and Hydrological Services and Regional Climate Centres and United Nations agencies, for their collaboration and input.

(Prof. Petteri Taalas)
Secretary-General

Global climate indicators

The global climate indicators provide an overview of changes in the climate system.[1] The set of interlinked physical indicators presented here connect the changing composition of the atmosphere with changes in energy in the climate system and the response of land, ocean and ice.

The global indicators are based on a wide range of data sets which comprise data from multiple observing systems including satellites and in situ networks (for details on data sets used in the report, see Data sets and methods).

The present report makes numerous references to the Working Group I contribution to the IPCC Sixth Assessment Report[2] (hereinafter referred to as IPCC AR6 WG I) and the IPCC Special Report on the Ocean and Cryosphere in a Changing Climate.[3]

BASELINES

Baselines are periods of time, usually spanning three decades or more, that are used as a fixed benchmark against which current conditions can be compared. For scientific, policy and practical reasons, a number of different baselines are used in this report, and these are specified in the text and figures. Where possible, the most recent WMO climatological standard normal, 1991–2020, is used for consistent reporting. This is the first year that the new normal, 1991–2020, has been used, and differences are described in Updating the climatological normal to 1991–2020.

For some indicators, however, it is not possible to use the standard normal owing to a lack of measurements during the early part of the period. For others – precipitation, for example – a longer period is required to calculate representative statistics. There are also two specific exceptions. First, for the global mean temperature time series – and *only* for the global mean series – a reference period of 1850–1900 is used. This is the baseline used in IPCC AR6 WG I as a reference period for pre-industrial conditions and is relevant for understanding progress in the context of the Paris Agreement. Second, greenhouse gas concentrations can be estimated much further back in time using gas bubbles trapped in ice cores. Therefore, the year 1750 is used in this report to represent pre-industrial greenhouse gas concentrations.

GREENHOUSE GASES

Atmospheric concentrations of greenhouse gases reflect a balance between emissions from human activities, natural sources and sinks. Increasing levels of greenhouse gases in the atmosphere due to human activities have been the major driver of climate change since at least the industrial revolution. Global average mole fractions of greenhouse gases – referred to here for simplicity as the "concentration" in the atmosphere – are calculated from in situ observations made at multiple sites through the Global Atmosphere Watch (GAW) Programme of WMO and partner networks.

---

[1] Trewin, B.; Cazenave, A.; Howell, S. et al. Headline Indicators for Global Climate Monitoring, *Bulletin of the American Meteorological Society* **2021** *102* (1), E20–E37. https://doi.org/10.1175/BAMS-D-19-0196.1.

[2] Intergovernmental Panel on Climate Change (IPCC), 2021: Summary for Policymakers. In: *AR6 Climate Change 2021: The Physical Science Basis*, https://www.ipcc.ch/report/ar6/wg1/downloads/report/IPCC_AR6_WGI_SPM_final.pdf.

[3] Intergovernmental Panel on Climate Change (IPCC), 2019: Summary for Policymakers. In: *IPCC Special Report on the Ocean and Cryosphere in a Changing Climate*, https://www.ipcc.ch/site/assets/uploads/sites/3/2022/03/01_SROCC_SPM_FINAL.pdf.

In 2021 – the latest year for which consolidated global figures are available – atmospheric levels of greenhouse gases reached new highs (Figure 1), with globally averaged surface mole fractions for carbon dioxide (CO_2) at 415.7 ± 0.2 parts per million (ppm), methane (CH_4) at 1908 ± 2 parts per billion (ppb) and nitrous oxide (N_2O) at 334.5 ± 0.1 ppb, respectively 149%, 262% and 124% of pre-industrial (1750) levels. Real-time data from specific locations, including Mauna Loa[4] (Hawaii, United States of America) and Kennaook/Cape Grim[5] (Tasmania, Australia) indicate that levels of CO_2, CH_4 and N_2O continued to increase in 2022.

The increase in CO_2 from 2020 to 2021 was equal to that observed from 2019 to 2020, but higher than the average annual growth rate over the last decade. While the long-term increase in CO_2 is due to human emissions, year-to-year variations in the rate are largely associated with natural variability in the land and ocean carbon sinks. The record annual increase in 2016 was associated with the strong 2015/2016 El Niño.[6]

The annual increase in CH_4 from 2020 to 2021 was 18 ppb. This is the largest annual increase on record, and its causes are still being investigated. Measurements of the atmospheric CH_4 burden and its stable carbon isotope ratio $^{13}C/^{12}C$ suggest that the largest contribution to the renewed increase in CH_4 since 2007 stems from microbial/biogenic sources, but the

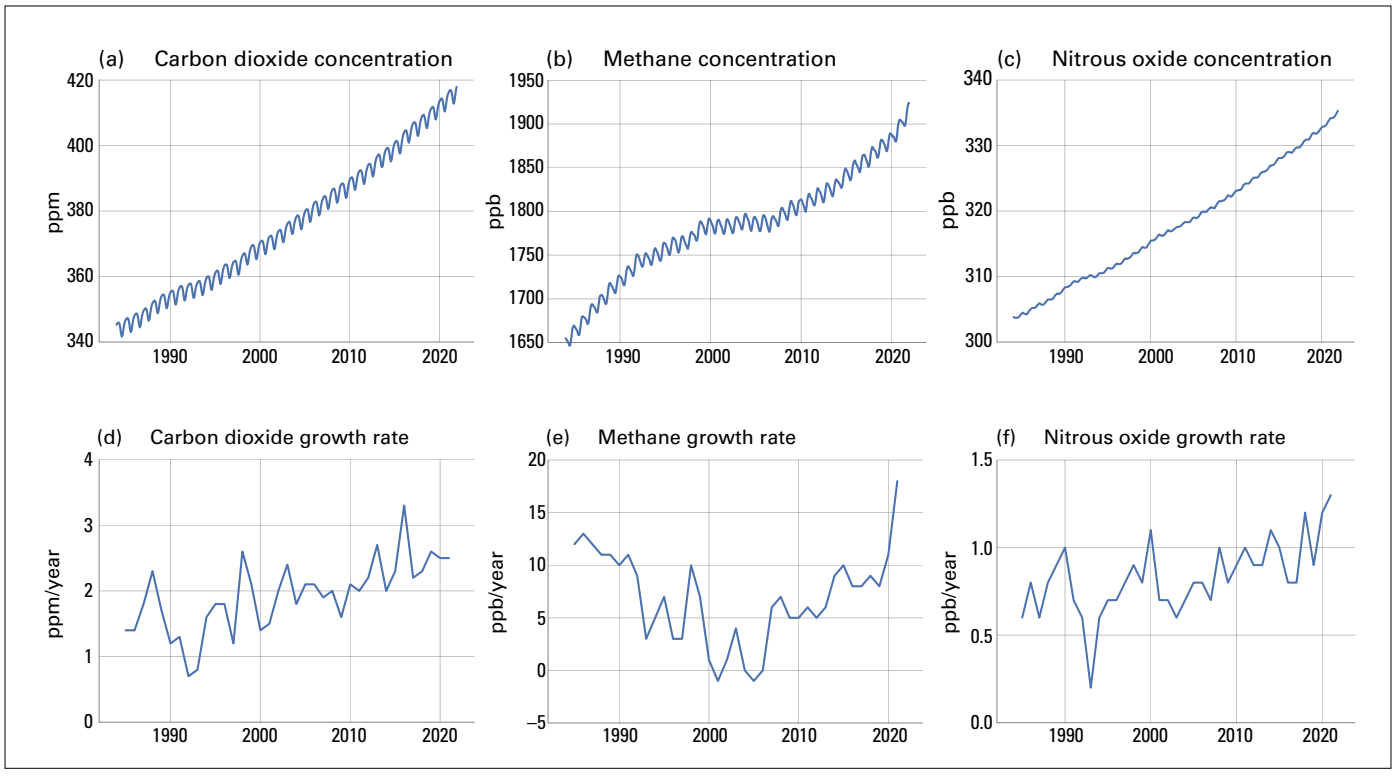

Figure 1. Top row: Monthly globally averaged mole fraction (measure of atmospheric concentration), from 1984 to 2021, of (a) CO_2 in parts per million, (b) CH_4 in parts per billion and (c) N_2O in parts per billion. Bottom row: the growth rates representing increases in successive annual means of mole fractions for (d) CO_2 in parts per million per year, (e) CH_4 in parts per billion per year and (f) N_2O in parts per billion per year.

[4] www.esrl.noaa.gov/gmd/ccgg/trends/mlo.html

[5] https://www.csiro.au/greenhouse-gases/

[6] Betts, R.; Jones, C.; Knight, J. et al. El Niño and a Record CO_2 Rise. *Nature Climate Change* **2016**, *6*, 806–810. https://doi.org/10.1038/nclimate3063.

relative roles of anthropogenic and natural sources are as yet unclear.[7,8] Improving observation networks in climate sensitive areas like tropical wetlands and the Arctic is a way to improve understanding of the processes that drive changes in GHGs. This knowledge could then be used to support efficient mitigation strategies.

TEMPERATURE

In 2022, the global mean temperature, which combines near-surface temperature measurements over land and ocean, was 1.15 [1.02–1.28] °C above the 1850–1900 pre-industrial average (Figure 2). The six data sets used in the analysis place 2022 as either the fifth or sixth warmest year on record (1850–2022). Differences between the data sets and hence in their rankings arise from differences in method and inaccuracies in the input data, and because some areas of the Earth remain sparsely observed. The years 2015 to 2022 are the eight warmest years on record in all data sets (for details see Data sets and methods).

La Niña conditions continued into a third year, having started in late 2020 (see Short-term climate drivers). La Niña is typically associated with a temporary reduction in global mean temperature, and both 2021 and 2022 were less warm than 2019 and 2020 due to the shift to La Niña conditions. Nonetheless, 2021 and 2022 were warmer than 2011 (when the global mean was 0.87 [0.74–0.99] °C above the 1850–1900 average), the last year to be affected by a significant La Niña event, and indeed warmer than any year prior to 2015. In most of the data sets, 2016, which was associated with an exceptionally strong El Niño, remains the warmest year on record globally (with a global mean 1.28 [1.15–1.40] °C above the 1850–1900 average).

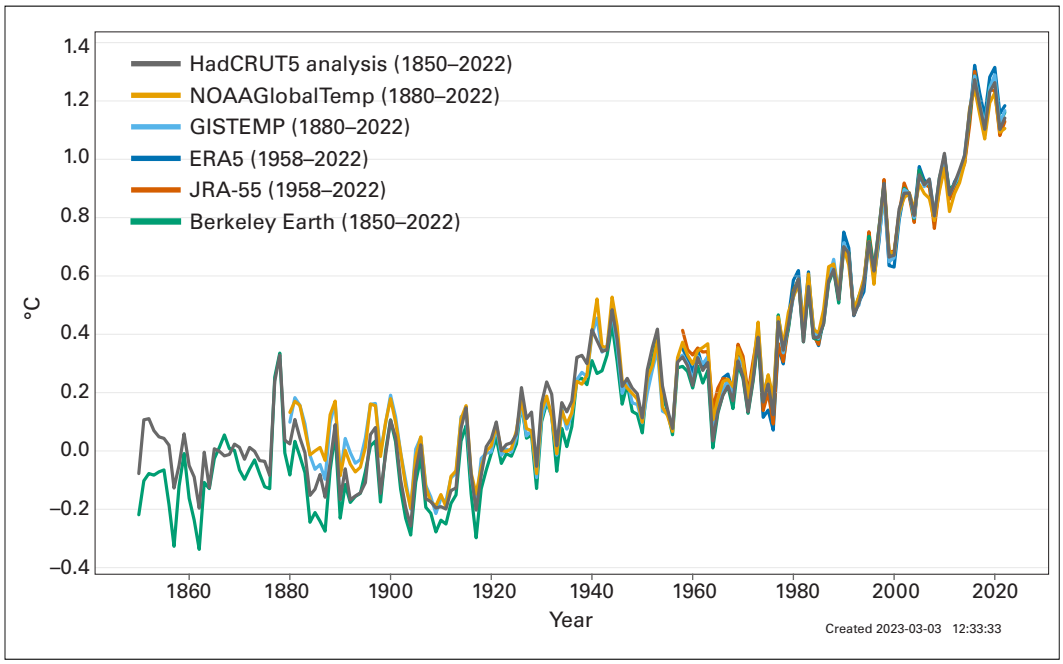

Figure 2. Global annual mean temperature anomalies with respect to pre-industrial conditions (1850–1900) for six global temperature data sets (1850–2022). For details of the data sets and processing see Data sets and methods.

[7] Lunt, M. F.; Palmer, P. I.; Feng, L., et al. An Increase in Methane Emissions from Tropical Africa Between 2010 and 2016 Inferred from Satellite Data. *Atmospheric Chemistry and Physics* **2019**, *19*, 14721–14740. https://doi.org/10.5194/acp-19-14721-2019.

[8] Feng, L.; Palmer, P. I.; Zhu, S. et al. Tropical Methane Emissions Explain Large Fraction of Recent Changes in Global Atmospheric Methane Growth Rate. *Nature Communications* **2022**, *13* (1), 1–8. https://doi.org/10.1038/s41467-022-28989-z.

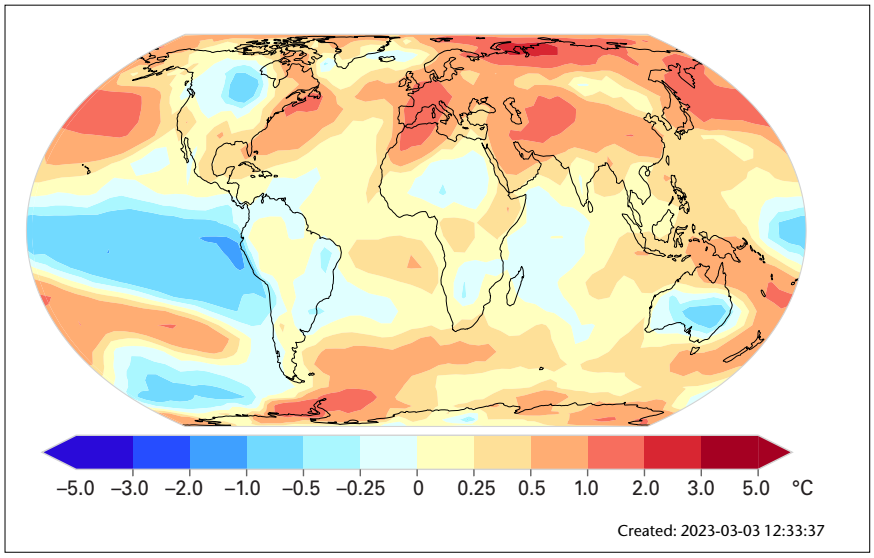

Figure 3. Near-surface temperature differences between 2022 and the 1991–2020 average. The map shows the median anomaly calculated from six data sets. For details on the data sets and processing, see Data sets and methods.

In the IPCC AR6 WG I report, long-term warming was assessed using multi-year averages.[9] For the decade 2011–2020, the average temperature was estimated to be 1.09 [0.95–1.20] °C above the 1850–1900 average. The 10-year average for the period 2013–2022 based on the data sets used here is estimated to be 1.14 [1.02–1.27] °C, indicating continued warming.

Over land (Figure 3), record high annual temperatures were reported in Western Europe (where a number of countries had their warmest year on record, including the United Kingdom of Great Britain and Northern Ireland, France, Ireland, Portugal, Spain, Belgium, Luxembourg, Italy, Germany and Switzerland), the western Mediterranean, parts of Central and Eastern Asia, and New Zealand. Over the ocean, record warmth extended across wide areas of the North and South Pacific as well as areas of the Southern Ocean.

No areas experienced record-low annual temperatures in 2022 (Figure 3). Conditions were colder than the 1991–2020 average in Canada, parts of Southern and Northern Africa, parts of Australia (New South Wales had its coolest year since 1996) and parts of South America. La Niña is associated with a "cold tongue" of cooler-than-average surface waters in the central and eastern equatorial Pacific, which is typically surrounded by areas of warmer-than-average waters running from the North Pacific, along the western rim and down into the South-west Pacific. In 2022, record warmth was measured over large areas of the North and South-west Pacific.

OCEAN

Covering around 70% of the Earth's surface, the ocean is an important part of the climate system. It absorbs both CO_2 and heat, thus slowing the pace of global warming in the atmosphere. At the same time, the resulting changes in chemistry and temperature have profound effects, reducing the pH of the ocean, raising sea level, changing ocean currents, and affecting sea life and biodiversity as well as the people who depend on the ocean for their livelihoods.[10]

[9] IPCC AR6 WG I used four data sets: HadCRUT5, NOAA Interim, Berkeley Earth and Kadow et al.

[10] Cheng, L.; von Schuckmann, K.; Abraham, J.P. et al. Past and Future Ocean Warming. *Nature Reviews Earth and Environment* **2022**, *3*, 776–794. https://doi.org/10.1038/s43017-022-00345-1.

OCEAN HEAT CONTENT

Increasing human emissions of CO_2 and other greenhouse gases cause a positive radiative imbalance at the top of the atmosphere leading to an accumulation of energy in the form of heat in the Earth system that is driving global warming.[11,12] Around 90% of the accumulated heat is stored in the ocean, leading to ocean warming. Ocean heat content (OHC) is an indicator that measures the accumulated heat. A positive energy imbalance signals that the climate is still responding to the current forcing and that more warming will occur even if the forcing does not increase further.[13] In a recent report the IPCC concluded that "It is *virtually certain* that the global upper ocean (0–700 m) has warmed since the 1970s and *extremely likely* that human influence is the main driver."[14]

The upper 2 000 m of the ocean continued to warm in 2022,[15] and it is expected that it will continue to warm in the future, causing changes that are irreversible on centennial to millennial time scales.[16,17] OHC in 2022 was the highest on record (Figure 4), exceeding the 2021 value

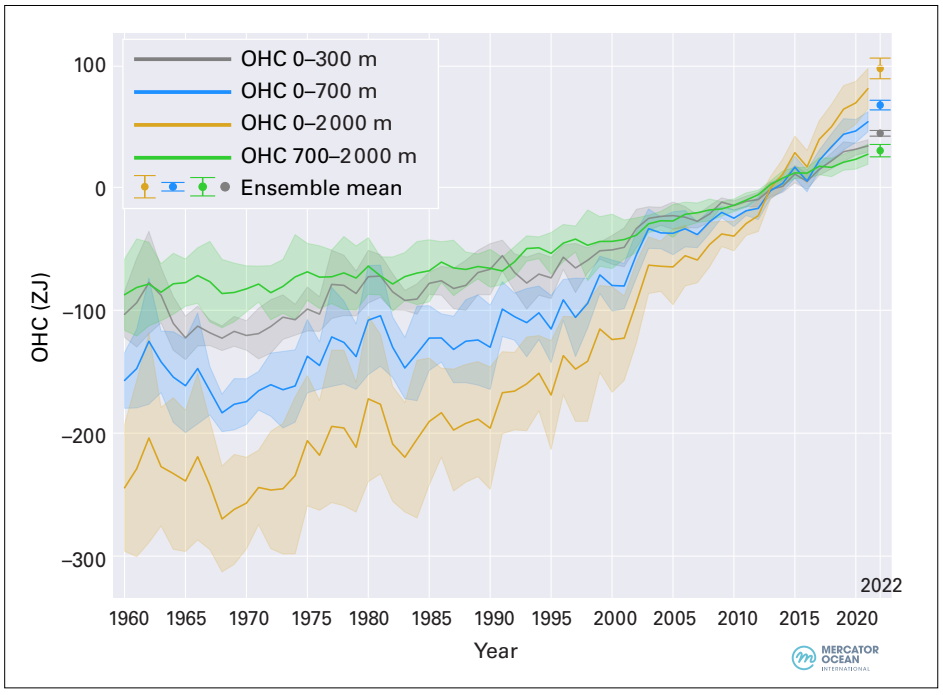

Figure 4. 1960–2021 ensemble mean time series and ensemble standard deviation (2 standard deviations, shaded) of global OHC anomalies relative to the 2005–2021 average for the 0–300 m (grey), 0–700 m (blue), 0–2 000 m (yellow) and 700–2 000 m (green) depth layers. The ensemble mean is an update of the outcome of a concerted international effort (see von Schuckmann, K.; Minère, A.; Gues, F. et al. Heat Stored in the Earth System 1960–2020: Where Does the Energy Go? *Earth System Science Data* **2022** [preprint]. https://doi.org/10.5194/essd-2022-239) and all products used are referenced in the section on Data sets and methods. Note that values are given for the ocean surface area between 60°S and 60°N and limited to areas deeper than 300 m in each product. The ensemble-mean OHC anomalies for the year 2022 have been added as separate points, together with their ensemble spread, and are based on the eight products listed in Data sets and methods.

Source: Mercator Ocean International.

[11] Hansen, J.; Sato, M.; Kharecha, P. et al. Earth's Energy Imbalance and Implications. *Atmospheric Chemistry and Physics* **2011**, *11* (24), 13421–13449. https://doi.org/10.5194/acp-11-13421-2011.

[12] von Schuckmann, K.; Palmer, M. D.; Trenberth, K. E. et al. An Imperative to Monitor Earth's Energy Imbalance. *Nature Climate Change* **2016**, *6*, 138–144. https://doi.org/10.1038/nclimate2876.

[13] Hansen, J.; Nazazarenko, L.; Ruedy, R. et al. Earth's Energy Imbalance: Confirmation and Implications. *Science* **2005**, *308* (5727), 1431–1435. https://doi.org/10.1126/science.1110252.

[14] Intergovernmental Panel on Climate Change (IPCC), 2021: Summary for Policymakers. In: *AR6 Climate Change 2021: The Physical Science Basis*, https://www.ipcc.ch/report/ar6/wg1/downloads/report/IPCC_AR6_WGI_SPM_final.pdf.

[15] von Schuckmann, K.; Cheng, L.; Palmer, M. D. et al. Heat Stored in the Earth System: Where Does the Energy Go? *Earth System Science Data* **2020**, *12* (3), 2013–2041. https://doi.org/10.5194/essd-12-2013-2020.

[16] Cheng, L.; Trenberth, K. E.; Fasullo, J. et al. Improved Estimates of Ocean Heat Content from 1960 to 2015. *Science Advances* **2017**, *3* (3), e1601545. https://doi.org/10.1126/sciadv.1601545.

[17] Intergovernmental Panel on Climate Change (IPCC), *IPCC Special Report on the Ocean and Cryosphere in a Changing Climate*, https://www.ipcc.ch/site/assets/uploads/sites/3/2022/03/01_SROCC_SPM_FINAL.pdf.

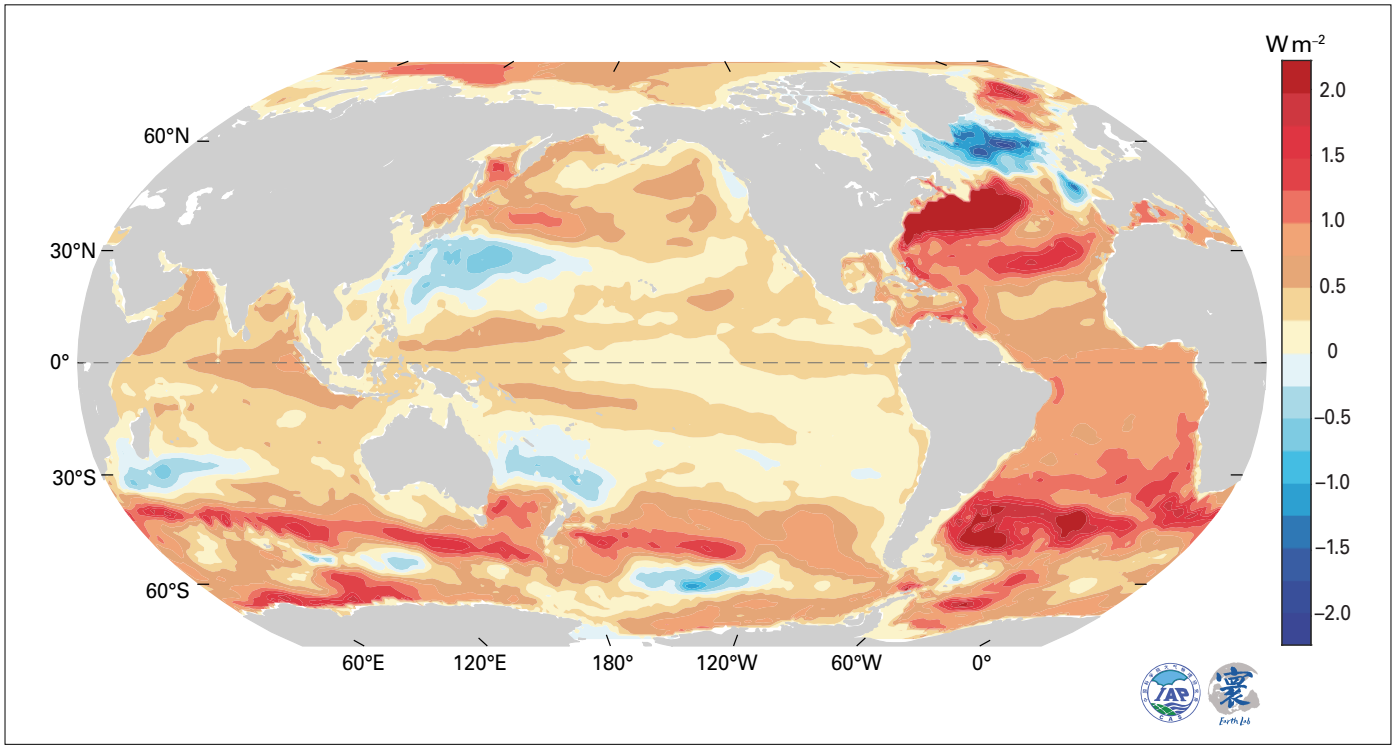

Figure 5. Estimated trend (W m^{-2}) in observed annual upper 2 000 m OHC from 1958 to 2022.

Source: Data updated from Cheng, L.; Trenberth, K. E.; Fasullo, J. et al. Improved Estimates of Ocean Heat Content from 1960 to 2015. *Science Advances* **2017**, *3* (3), e1601545. https://doi.org/10.1126/sciadv.1601545.

by 17 ± 9 ZJ[18] . All data sets agree that ocean warming rates were particularly high in the past two decades: the rate of ocean warming for 0–2 000 m was 0.7 ± 0.1 W m^{-2} from 1971 to 2022, but 1.2 ± 0.2 W m^{-2} from 2006 to 2022. Deep ocean warming below a depth of 2 000 m is estimated to have been 0.0725 ± 0.1 W m^{-2} from 1992 to 2022.

Although global mean OHC has increased strongly, the rate of ocean warming has not been the same everywhere.[19] The strongest warming in the upper 2 000 m occurred in the Southern Ocean, North Atlantic and South Atlantic, where warming locally exceeded 2 W m^{-2} (Figure 5). The Southern Ocean is the largest reservoir of heat, accounting for around 36% of the global OHC increase in the upper 2 000 m since 1958. This strong warming is associated with the absorption of anthropogenic heat by the cold upwelling waters which is then exported to the northern edge of the Antarctic Circumpolar Current by the background overturning circulation.

Some limited regions are losing heat and are cooling, including the subpolar Atlantic Ocean extending from near the surface down to >800 m depth (also the only area to show centennial cooling at the surface). The contrasting pattern of cooling (50°N–70°N) and warming (20°N–50°N) in the North Atlantic is associated with a slowing of the Atlantic Meridional Overturning Circulation and local interactions between the air and sea.

[18] Ocean heat content is measured in zettajoules. A zettajoule is 10^{21} joules, which is 1 000 000 000 000 000 000 000 joules.

[19] Cheng, L.; von Schuckmann, K.; Abraham, J. P. et al. Past and Future Ocean Warming. *Nature Reviews Earth and Environment* **2022**, *3*, 776–794. https://doi.org/10.1038/s43017-022-00345-1.

SEA LEVEL

Global mean sea level (GMSL) continued to rise in 2022 (Figure 6). The GMSL rise is estimated to be 3.4 ± 0.3 mm yr^{-1} over the 30 years of the satellite altimeter record (1993–2022), but the rate has doubled between the first decade of the record (1993–2002) and the last (2013–2022), during which the rate has exceeded 4 mm yr^{-1}. The acceleration in GMSL is estimated to be 0.12 ± 0.05 mm yr^{-2} over the 30-year period. Sea level rise is not the same everywhere, with the differences due in part to local changes in OHC (Figure 7).

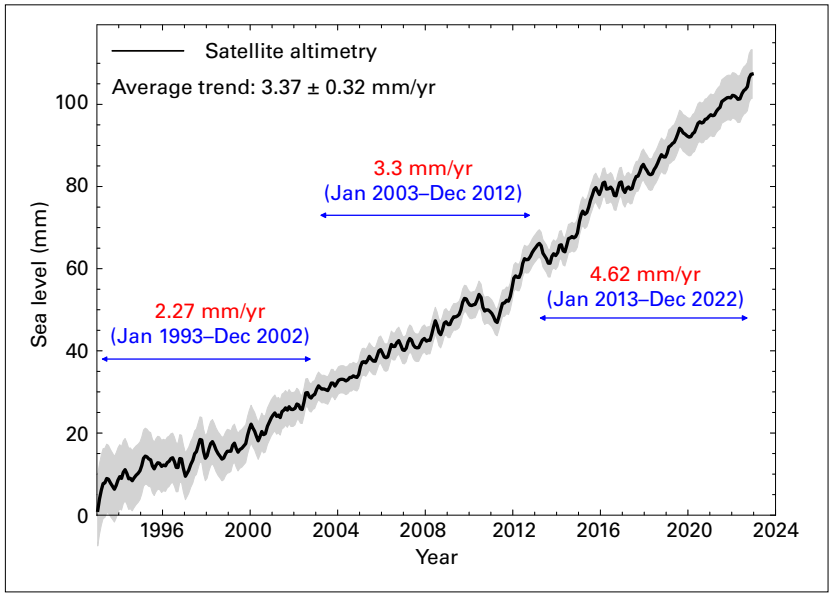

Figure 6. GMSL evolution from January 1993 to December 2022 (black curve) with associated uncertainty (shaded area) based on satellite altimetry. The horizontal, coloured lines represent the average linear trends over three successive time spans.

Source: Laboratoire d'Etudes en Géophysique et Océanographie Spatiales (LEGOS); data from AVISO altimetry (https://www.aviso.altimetry.fr).

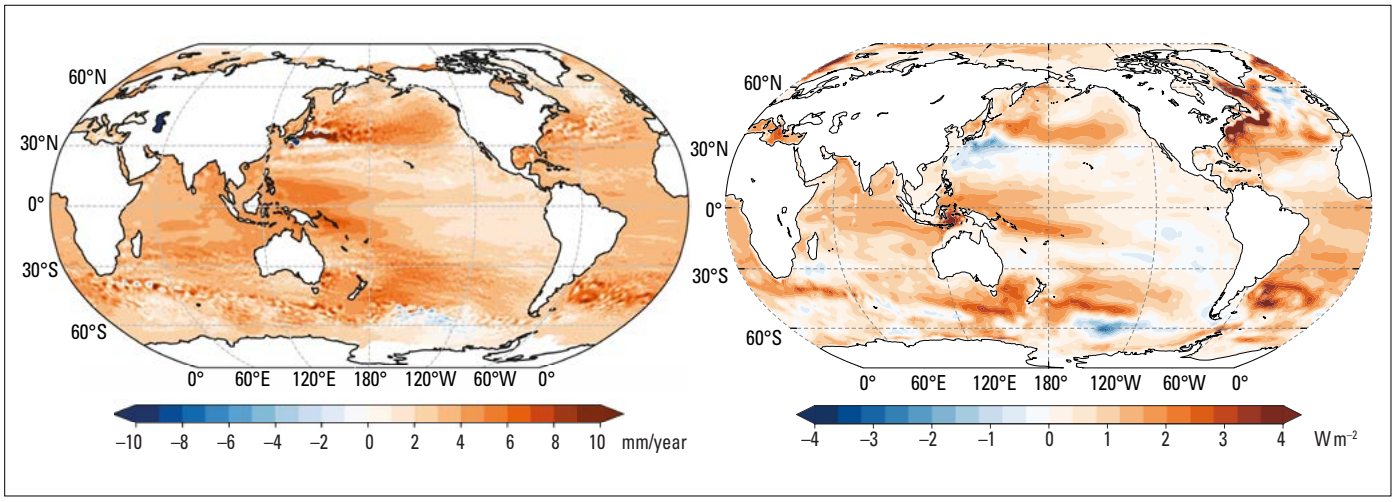

Figure 7. Left: Sea-level trends (mm yr^{-1}) for the period 1993–2022.

Source: LEGOS, data from the Copernicus Climate Change Service (https://climate.copernicus.eu).

Right: OHC trends (W m^{-2}) for 0–2 000 m depth for the period 1993–2022.

Source: Data updated from Cheng, L.; Trenberth, K. E.; Fasullo, J. et al. Improved Estimates of Ocean Heat Content from 1960 to 2015. *Science Advances* **2017**, *3* (3), e1601545. https://doi.org/10.1126/sciadv.1601545.

Ocean warming, ice loss from glaciers and ice sheets, and changes in land water storage all contribute to changes in sea level. The GMSL budget compares the sum of estimates of the individual components to the total GMSL measured by satellites. If the sum of the estimates matches the total GMSL, the budget is said to be "closed". The budget has recently been updated,[20] and the GMSL budget can now be closed to the end of 2020 within data uncertainties (Figure 8). For the period 2005–2019 where individual mass contributions can be estimated, total land ice loss from glaciers, Greenland and Antarctica contributed 36% to the GMSL rise, and ocean warming (through thermal expansion) contributed 55%. Variations in land water storage contributed less than 10%.

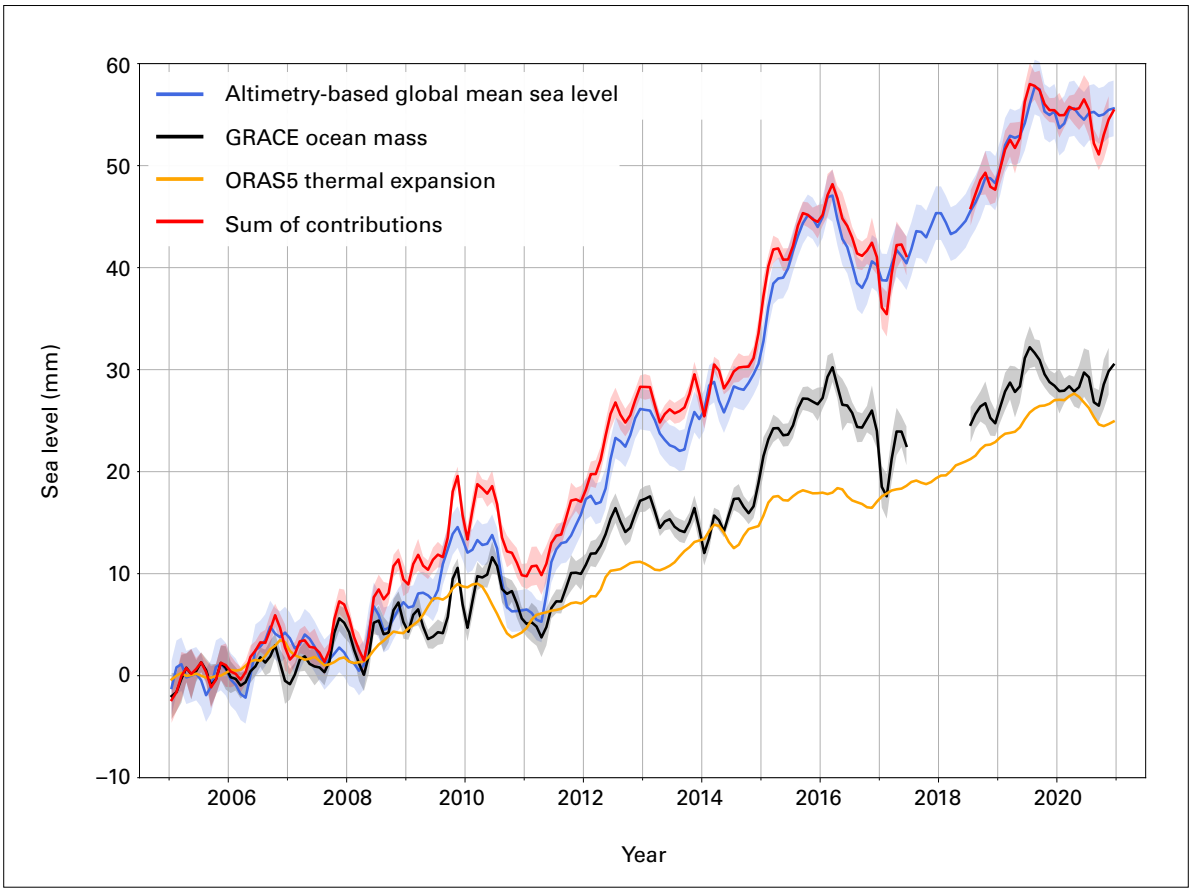

Figure 8. GMSL budget between January 2005 and December 2020. The Jason-3 data used for the GMSL as of 2008 are corrected for the onboard radiometer drift. Note that the mask applied to the sea-level data is different from that used in Figure 6, so some details may differ. GRACE-based ocean mass is an ensemble mean of six different solutions. The thermal expansion is based on the ORAS5 reanalysis.

Source: Barnoud A., Pfeffer J., Cazenave A. et al. Revisiting the global ocean mass budget over 2005-2020. *Ocean Sciences*, **2023**, *19* (2), 321–334. https://doi.org/10.5194/os-19-321-2023.

[20] Barnoud, A.; Pfeffer, J.; Cazenave, A. et al. Revisiting the Global Mean Ocean Mass Budget over 2005–2020. *Ocean Sciences* **2023**, *19* (2), 321–334. https://doi.org/10.5194/os-19-321-2023.

MARINE HEATWAVES AND COLD SPELLS

As with heatwaves and cold spells on land, marine heatwaves (MHWs) and marine cold spells (MCSs) are prolonged periods of extreme heat or cold in the seas and oceans that can have a range of consequences for marine life and dependent communities.[21] MHWs have become more frequent over the late twentieth and early twenty-first centuries (Figure 9(d)), while MCSs have become less frequent (Figure 10(d)). Satellite retrievals of sea-surface temperature (SST) are used to monitor MHWs and MCSs globally, categorized here as *moderate*, *strong*, *severe* or *extreme* (for definitions, see Data sets and methods).

Overall, 58% of the ocean surface experienced at least one MHW during 2022 (Figure 9(d)) – less than the record of 65% in 2016 and similar to 2021 (57%). In total, 25% of the ocean surface experienced at least one MCS during 2022, similar to 2021 (25%) and much less than the 1985 record (63%).

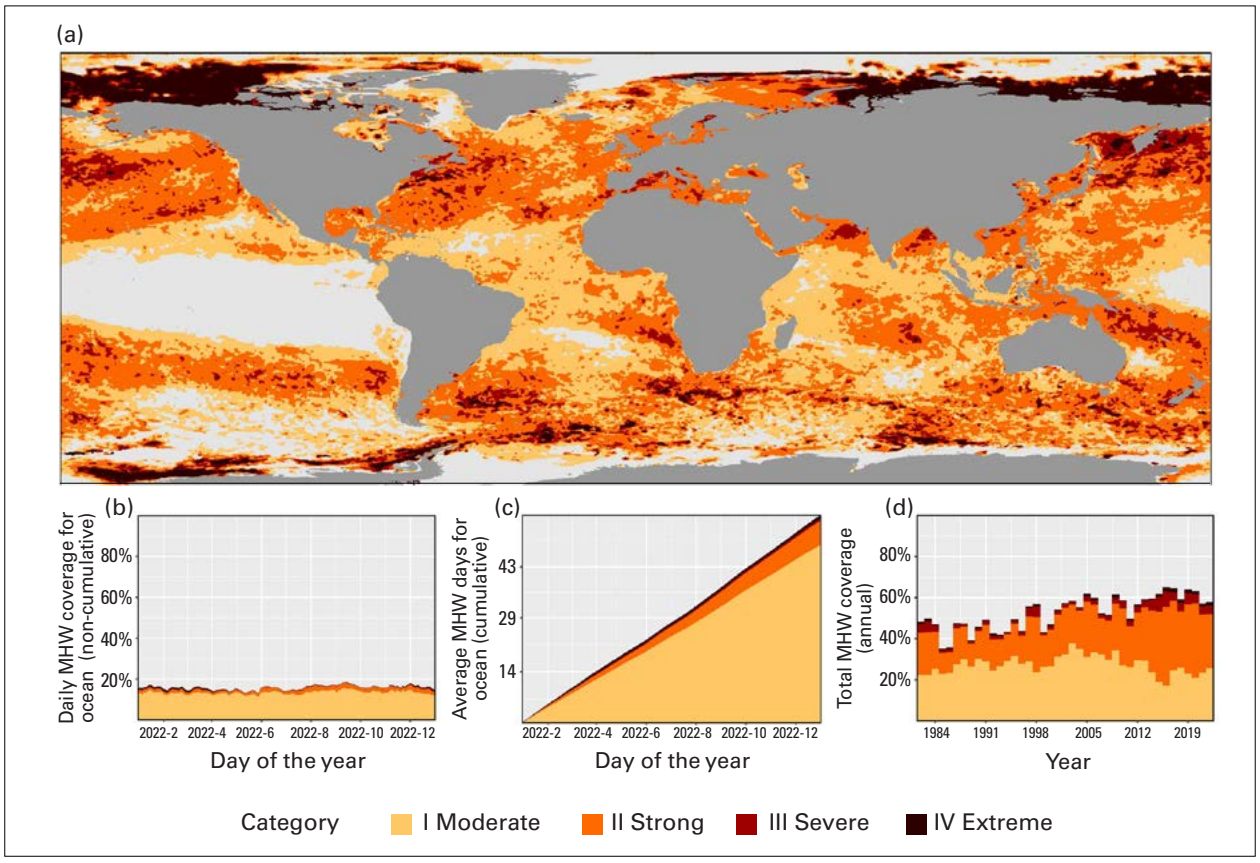

Figure 9. (a) Global map showing the highest MHW category (for definitions, see Data sets and methods) experienced at each pixel (resolution is 0.25° x 0.25°) over 2022 (reference period 1982–2011). Light grey indicates that no MHW occurred in a pixel over the entire year. (b) Stacked bar plot showing the percentage of the surface of the ocean experiencing an MHW on any given day of the year. (c) Stacked bar plot showing the cumulative number of MHW days averaged over the surface of the ocean. Note: The average is calculated by dividing the cumulative sum of MHW days per pixel weighted by the surface area of those pixels. (d) The annual total surface area of the ocean that experienced a MHW from 1982 to 2022. Data are from the National Oceanic and Atmospheric Administration Optimum Interpolation Sea Surface Temperature (NOAA) OISST.

Source: Robert Schlegel.

[21] Smith, K. E.; Burrows, M. T.; Hobday, A. J. et al. Biological Impacts of Marine Heatwaves. *Annual Review of Marine Science* **2023**, 15 (1), 119–145. https://doi.org/10.1146/annurev-marine-032122-121437.

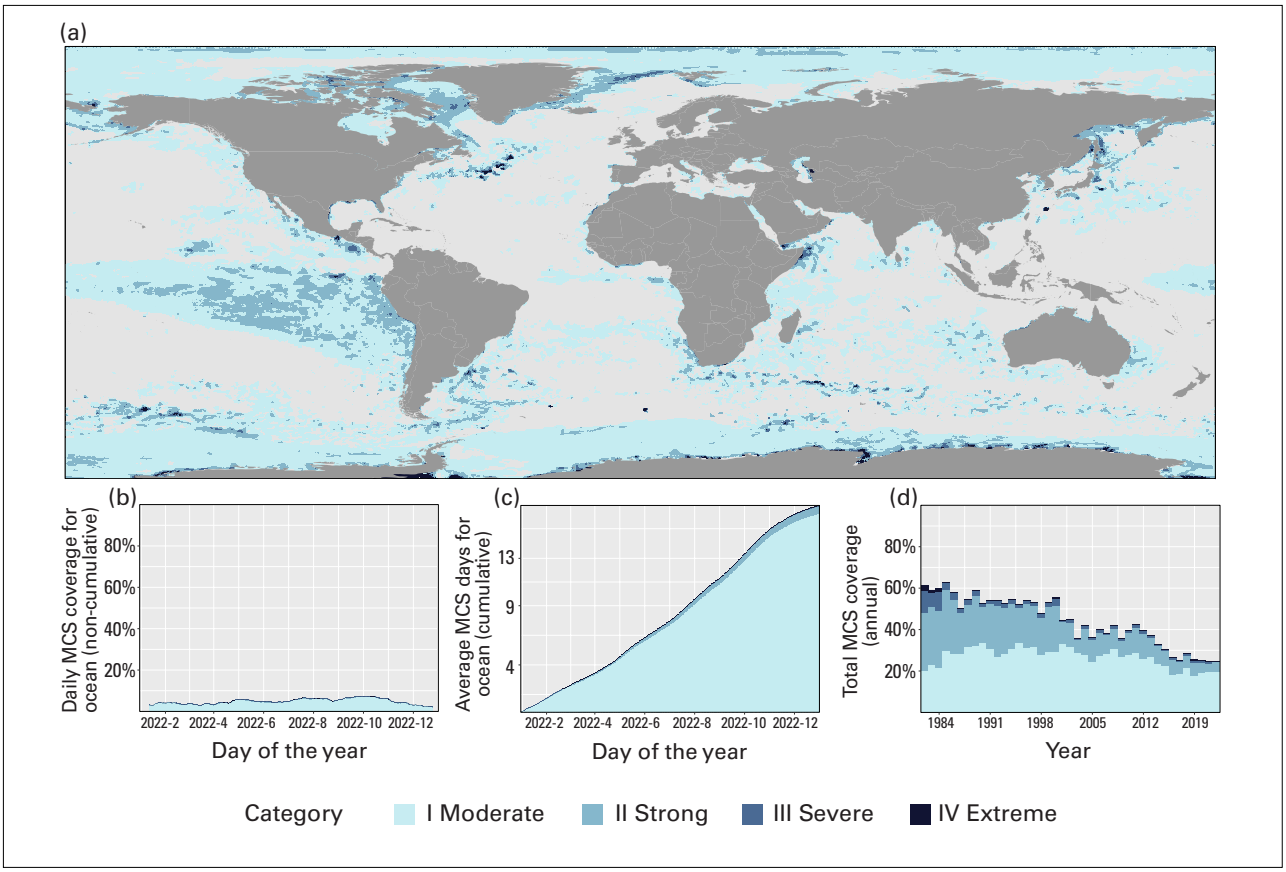

Figure 10. As for Figure 9 but showing MCSs rather than MHWs. Data are from NOAA OISST.

Source: Robert Schlegel.

La Niña and associated lower-than-average SSTs mean that the equatorial Pacific was one of the few ocean regions to see widespread *strong* MCSs in 2022 (Figure 10). The Southern Ocean is, however, the only region in which there have been long-term increases in the duration of MCSs, albeit over limited areas.[22] In the Arctic, the Laptev and Beaufort Seas experienced *severe* and *extreme* MHWs from spring to autumn of 2022. The ice edges to the north of Svalbard and to the east of the Ross Sea experienced notable *extreme* MHWs for the second consecutive year.

OCEAN ACIDIFICATION

Between 1960 and 2021, the ocean absorbed around 25% of the annual emissions of anthropogenic CO_2 to the atmosphere, thereby helping to partially alleviate the impacts of climate change.[23] However, the negative impacts on the ocean are high; CO_2 reacts with seawater, resulting in a decrease of pH referred to as ocean acidification. Ocean acidification threatens

[22] Wang, Y.; Kajtar, J. B.; Alexander, L. V. et al. Understanding the Changing Nature of Marine Cold-spells. *Geophysical Research Letters* **2022**, *49*, e2021GL097002. https://doi.org/10.1029/2021GL097002.

[23] Friedlingstein, P.; O'Sullivan, M.; Jones, M. W. et al. Global Carbon Budget 2022, *Earth System Science Data* **2022**, *14*, 4811–4900. https://doi.org/10.5194/essd-14-4811-2022.

organisms and ecosystem services.[24] As the acidity and temperature of the ocean increases, its capacity to absorb CO_2 from the atmosphere decreases, potentially impeding the ocean's role in moderating climate change.[25] The importance of ocean acidification is reflected in Sustainable Development Goal (SDG) Indicator 14.3.1,[26] and global efforts are underway to monitor ocean acidification.

The limited number of long-term observations in the open ocean have shown a decline in pH (Figure 11, left), with a change in average global surface ocean pH of 0.017–0.027 pH units per decade since the late 1980s.[27] The IPCC AR6 concluded that "There is very high confidence that open ocean surface pH is now the lowest it has been for at least 26 [thousand years] and current rates of pH change are unprecedented since at least that time".[28] Observations of ocean acidification from coastal areas present a more varied picture (Figure 11, right), due to the complex interplay of factors such as freshwater influx, biological activity and anthropogenic influences in coastal seas.

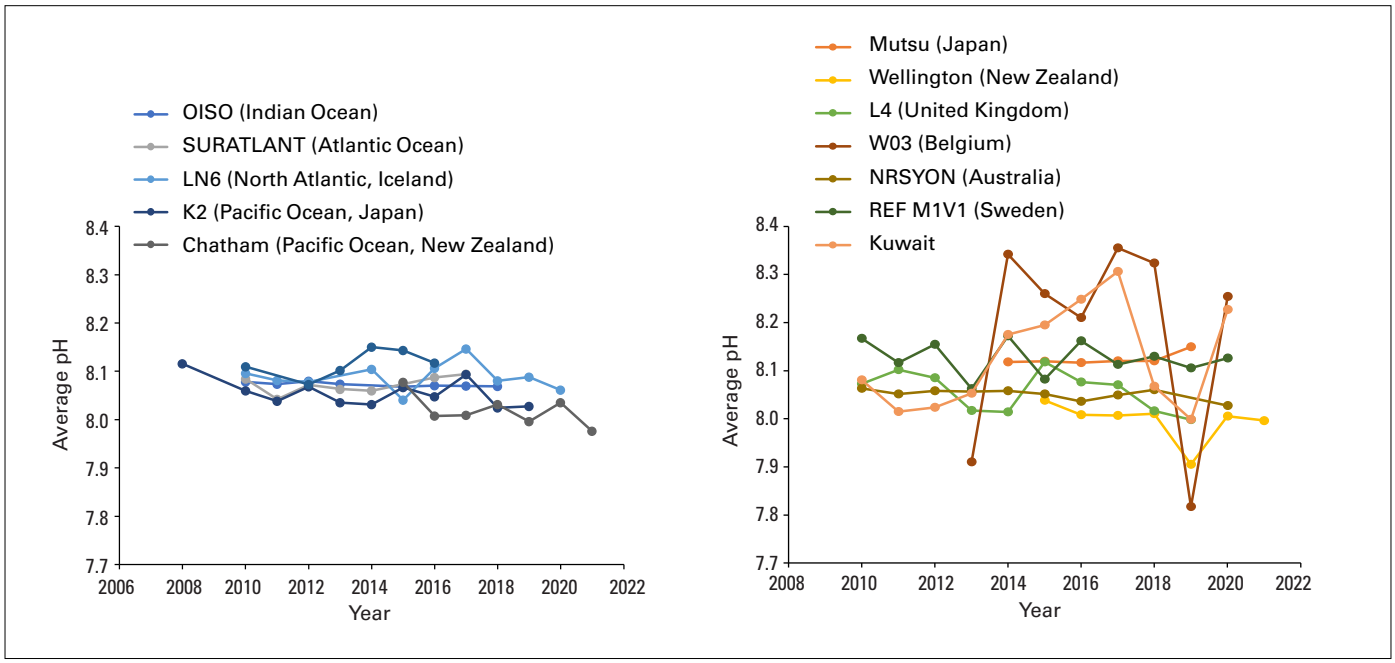

Figure 11. Variations in the annual average pH values from a suite of representative sampling stations in open waters, 2008–2021 (left), and in coastal waters, 2010–2021 (right). For station details see Data sets and methods.

Source: IOC/UNESCO.

[24] Intergovernmental Panel on Climate Change (IPCC), 2019, *IPCC Special Report on the Ocean and Cryosphere in a Changing Climate,* https://www.ipcc.ch/site/assets/uploads/sites/3/2022/03/01_SROCC_SPM_FINAL.pdf.

[25] Gruber, N.; Bakker, D. C. E.; DeVries, T. et al. Trends and Variability in the Ocean Carbon Sink. *Nature Reviews Earth and Environment* **2023** *4*, 119–134. https://doi.org/10.1038/s43017-022-00381-x.

[26] The SDG Indicator 14.3.1 is under the custodianship of the Intergovernmental Oceanographic Commission (IOC) of the United Nations Educational, Scientific and Cultural Organization (UNESCO).

[27] Intergovernmental Panel on Climate Change (IPCC), 2019, *IPCC Special Report on the Ocean and Cryosphere in a Changing Climate,* https://www.ipcc.ch/site/assets/uploads/sites/3/2022/03/01_SROCC_SPM_FINAL.pdf.

[28] Intergovernmental Panel on Climate Change (IPCC), 2021: Climate Change 2021: The Physical Science Basis, Chapter 2, section 2.3.3.5 Ocean pH, https://www.ipcc.ch/report/ar6/wg1/.

CRYOSPHERE

The cryosphere comprises the frozen parts of the Earth – glaciers and ice sheets, sea ice, snow and permafrost. The inhospitable and often remote environments in which they form mean that it has sometimes been challenging to undertake long-term measurements of these phenomena.

SEA ICE

Arctic sea-ice extent in 2022 was below the 1991–2020 average for most of the year, with a spring sea-ice monthly maximum of 14.59 million km² in March 2022, 0.44 million km² below the long-term mean (Figure 12). The monthly minimum extent in September was 4.87 million km², 0.71 million km² lower than the long-term mean. The minimum ice extent was greater than the average minimum values of the last decade (2012–2021) – consistent with a moderate summer for Arctic sea-ice melt – but is still tied for the eleventh lowest monthly minimum ice extent in the satellite record. The smallest daily extent of the year, 4.67 million km², occurred on 18 September 2022 and tied for the tenth lowest annual minimum daily extent on record.[29]

Sea-ice extent in the Antarctic has seen both record highs (2014) and record lows (2017/2022) in the past 10 years. Antarctic sea-ice extent dropped to 1.92 million km² on 25 February 2022, the lowest level on record and almost 1 million km² below the long-term (1991–2020) mean.[30] The origins of the ice loss can be traced back to October/November 2021 when there was a series of storms to the west of the Antarctic Peninsula. This area is strongly influenced by the El Niño–Southern Oscillation (ENSO), and the storms are consistent with La Niña conditions

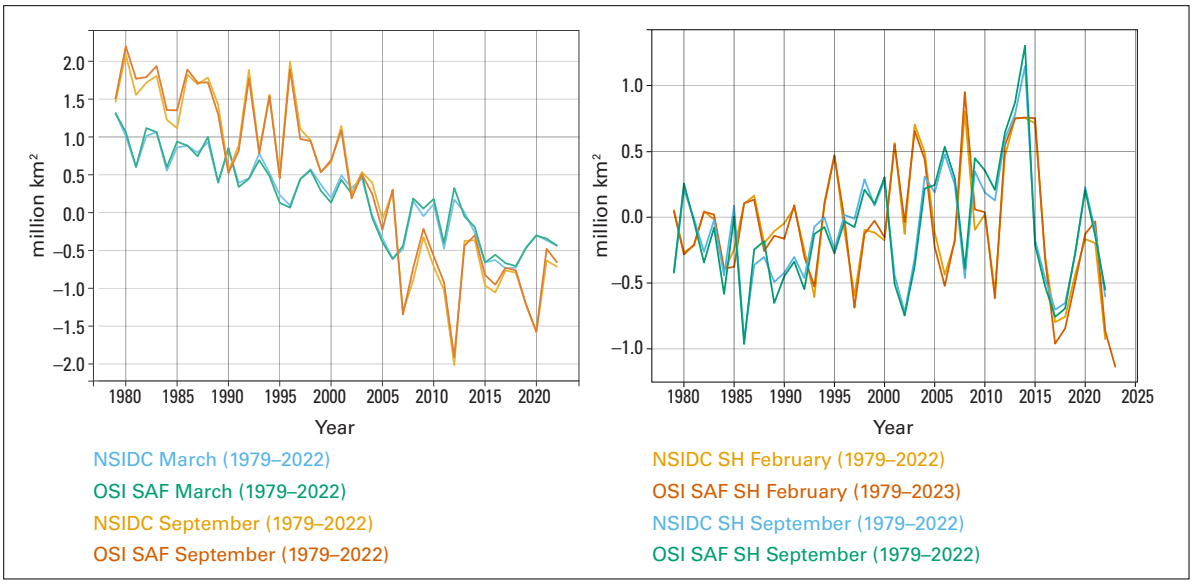

Figure 12. Sea-ice extent anomalies 1979 to 2022 (relative to the 1991–2020 average) for (left) the Arctic and (right) the Antarctic. Blue/green lines indicate the anomalies in annual maximum ice extent (March or September), and orange/red lines correspond to the annual minimum ice extent (September or February).

Source: Data from EUMETSAT OSI SAF v2p1 and National Snow and Ice Data Centre (NSIDC) v3 (Fetterer et al., 2017) (see details in Data sets and methods).

[29] https://nsidc.org/arcticseaicenews/2022/09/arctic-sea-ice-minimum-ties-tenth-lowest/

[30] Turner, J.; Holmes, C.; Caton Harrison, T. et al. Record Low Antarctic Sea Ice Cover in February 2022. *Geophysical Research Letters* **2022**, *49*, e2022GL098904. https://doi.org/10.1029/2022GL098904.

at the time. Southerly winds of up to 30 m s^{-1} moved sea ice away from the coast of West Antarctica, creating a 1 million km^2 area of open water known as a polynya. The exposed ocean warmed rapidly in the summer sun, leading to further sea-ice loss.

Following the annual sea-ice extent minimum in February, the total extent of Antarctic sea ice was continuously below the 30-year (1991–2020) mean up to the end of 2022, including periods with record lows in June and July. The maximum annual Antarctic sea-ice extent in October 2022 was 0.8 million km^2 below the mean maximum extent.

GLACIERS

Glaciers are formed from snow that has compacted to form ice, which then deforms and flows downhill to lower, warmer altitudes, where it melts. Where glaciers end in a lake or the ocean, ice loss also occurs through melting where the ice and water meet and via calving when chunks of the glacier fall off.

In the hydrological year 2021/2022, the approximately 40 glaciers with long-term observations monitored by the World Glacier Monitoring Service experienced an average mass balance of –1.18 m water equivalent (m w.e.).[31] This loss is much larger than the average over the last decade (Figure 13). The cumulative mass balance since 1970 amounts to over 26 m w.e. Strong regional differences were observed; record glacier melting occurred in the European Alps (see below), but there were some mass gains in Iceland and northern Norway associated with higher-than-average precipitation and a relatively cool summer. Measurements on glaciers in high-mountain Asia,[32] Western North America, South America and parts of the Arctic also

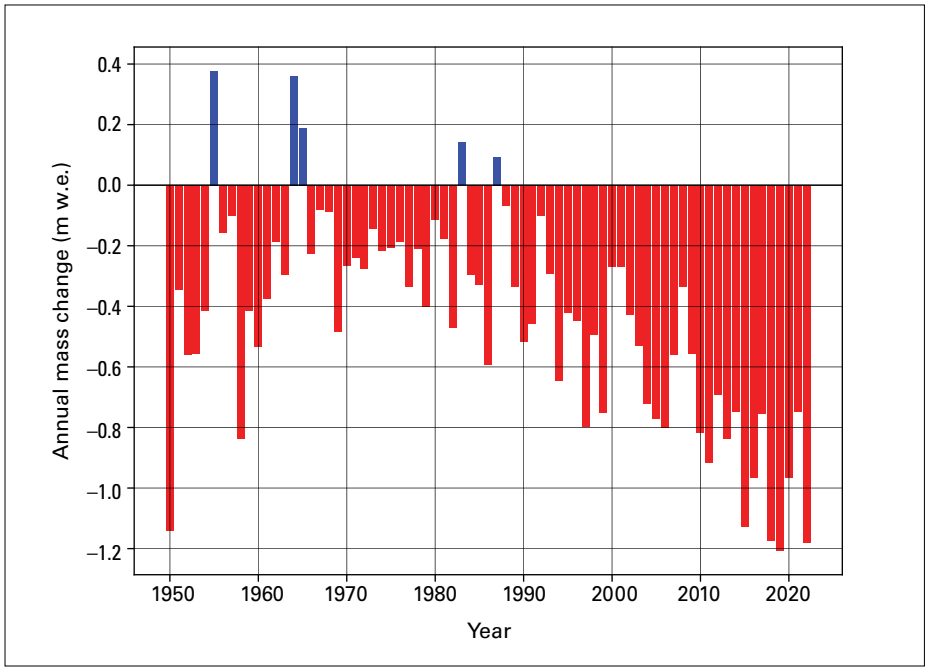

Figure 13. Global annual mass change of a composite of approximately 40 reference glaciers worldwide covering the period 1950–2022.

Source: Data provided by the World Glacier Monitoring Services (www.wgms.ch)

[31] The unit m w.e. represents the depth of water which would be obtained by melting the snow or ice and pouring it into the geographical area covered by the glaciers.

[32] High-mountain Asia refers to the high-altitude area in Asia including the Tibetan Plateau and extending from the Hindu Kush and Tien Shan in the west to the eastern-most extent of the Himalayas.

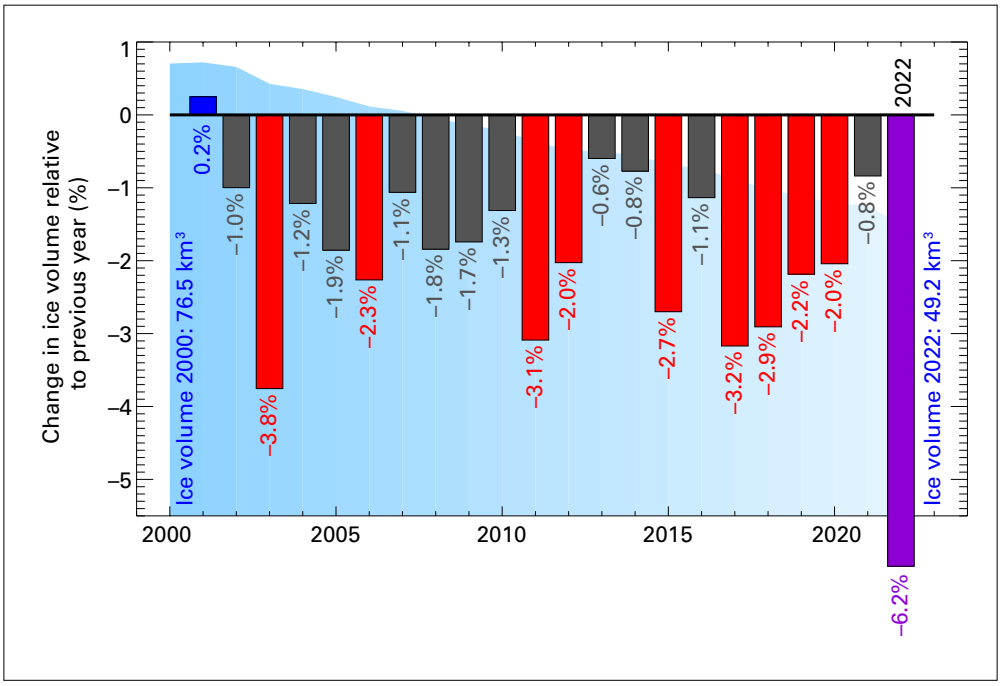

Figure 14. Total annual loss of Swiss glaciers related to the current ice volume 2002–2022. The vertical bars indicate the percentage change in ice volume relative to the previous year. Red and purple bars are the 10 largest relative mass losses on record. The purple bar is the relative mass loss for 2022. The blue shaded area in the background represents the overall ice volume.

Source: Matthias Huss based on Glacier Monitoring Switzerland, 2022: *Swiss Glacier Mass Balance (Release 2022)*, https://doi.org/10.18750/massbalance.2022.r2022.

reveal substantial glacier mass losses. The major glacier melt in most regions in 2022 is in line with the long-term acceleration of glacier mass losses, with six of the ten most negative mass balance years on record, including 2022, occurring since 2015.

In the European Alps, glacier mass loss records were broken by large margins in 2022. Mass losses were far beyond the range of historical variability.[33] Average thickness changes of 3 to over 4 metres were measured throughout the Alps, substantially more than in the previous record year of 2003. In Switzerland, 6% of glacier ice volume was lost between 2021 and 2022 (Figure 14). There are three reasons for this extreme glacier melt. First, there was very little winter snow, which meant that the ice was unprotected in early summer. Second, dust from the Sahara blew over the Alps in March 2022. The dust darkened the snow surface (reduced its albedo), which consequently absorbed more heat from the sun, further accelerating snow melt. Third, heat waves between May and early September 2022 led to massive ice loss. Snow on the glaciers started melting about one month earlier than usual and, for the first time in history, no snow survived the summer melt season even at the very highest measurement sites and thus no accumulation of fresh ice occurred. Between 2001 and 2022 the volume of glacier ice in Switzerland has decreased from 77 km^3 to 49 km^3, a decline of more than one third.

During the summer, the zero-degree line in the European Alps rose to over 5 000 metres above sea level. A weather balloon ascent at Payerne in Switzerland recorded 0 °C at a height of 5 184 m on 25 July, the highest in the 69-year record and only the second time that the height of the zero-degree line had exceeded 5 000 m.[34] New record temperatures were reported at the summit of Mont Blanc. Related to the heat, strong rockfall activity was observed, and an ice avalanche and glacier detachment triggered by meltwater at Marmolada, Italy, claimed the lives of 11 climbers.

[33] While the longest records exceed 100 years, systematic long-term observations at a number of other glaciers started in the 1950s.

[34] https://www.meteoschweiz.admin.ch/dam/jcr:f8acdbc9-ba7e-4ddb-ae70-8404f5374632/alpenklima_DE_20221205.pdf

Glaciers of Western North America experienced mass loss in 2022 in line with average mass balances over the last two decades. However, there were unusually negative mass balances in early autumn 2022 in this region (and in Greenland, see below), associated with high temperatures in September and October. In south-western Canada, glaciers remained snow free through these months and lost an additional ~0.6 m w.e. of ice, roughly doubling the net annual mass loss from these glaciers for the hydrological year September 2021–August 2022 after the season had finished. This mass loss is not captured in typical field campaigns, which survey changes at the end of the summer melt season, for example in early September.

ICE SHEETS

An ice sheet[35] is an area of ice on land that exceeds 50 000 km^2. In the current climate there are two ice sheets: the Greenland ice sheet and the Antarctic ice sheet. The total mass balance (TMB) of an ice sheet is the sum of three components: the surface mass balance (SMB), the marine mass balance (MMB) and the basal mass balance (BMB). The SMB is the difference between snow accumulation and meltwater runoff from the ice sheet. The MMB is the mass loss at the edge of the ice sheet from the calving of icebergs and the melting of ice that is in contact with the ocean. BMB consists of melting at the ice sheet bed due to geothermal heat and friction as the ice slides over the ground beneath it. A negative mass balance indicates a loss of ice mass; a positive mass balance indicates a gain.

For the Greenland ice sheet,[36] the estimated TMB in the 2022 mass balance year (1 September 2021 to 31 August 2022) was –85 Gt,[37] a net ice loss. The 2021–2022 SMB was about 420 Gt, which is the tenth highest value in the dataset (1980–2022) (Figure 15). Nevertheless, the Greenland ice sheet ended with a negative TMB for the twenty-sixth year in a row, mainly

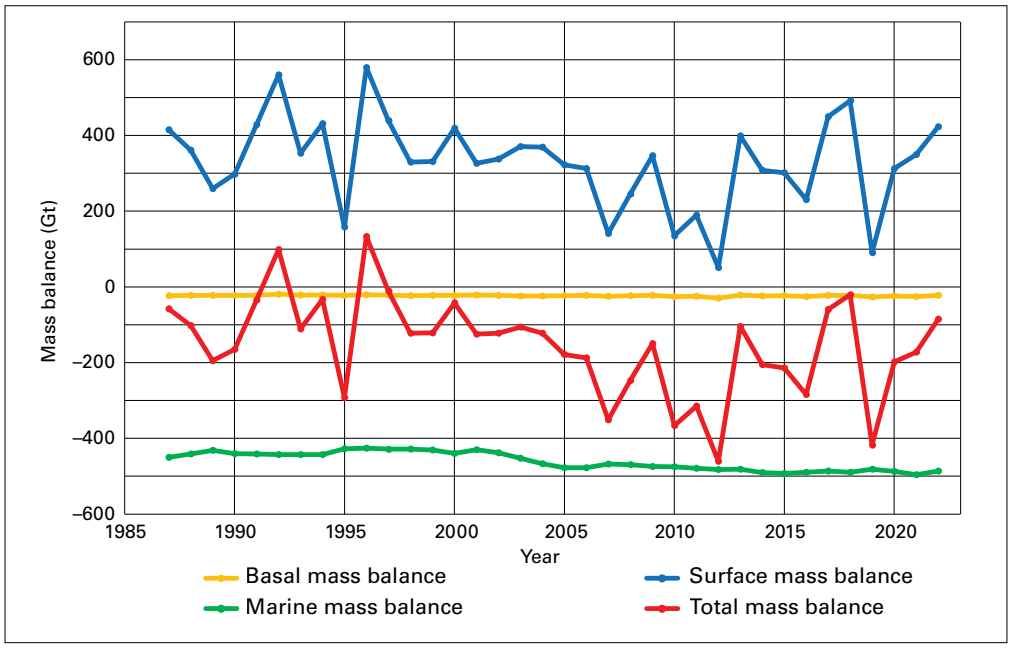

Figure 15. Components of the total mass balance (TMB) of the Greenland ice sheet 1987–2022. Blue: surface mass balance (SMB); green: marine mass balance (MMB); orange: basal mass balance (BMB); red: TMB, the sum of SMB, MMB and BMB.

Source: Mankoff et al. (2021), updated by M. Stendel, DMI.

[35] https://www.ipcc.ch/srocc/chapter/glossary/

[36] Based on the average of three regional climate and mass balance models. See Mankoff, K. D.; Fettweis, X.; Langen, P.L. et al. Greenland Ice Sheet Mass Balance from 1840 through Next Week. *Earth System Science Data* **2021**, *13*, 5001–5025. https://doi.org/10.5194/essd-13-5001-2021

[37] A gigatonne (Gt) is 1 000 000 000 tonnes, and 1 Gt of ice corresponds to a volume of around 1.09 km^3.

due to the strong negative MMB of –480 Gt. An independent measure of the TMB has been available since 2002 based on the GRACE and GRACE Follow-on (FO) satellite missions. The GRACE-FO data indicate a TMB of –305 Gt (Figure 17(a)), a much larger mass loss than the estimate of –85 Gt from the regional mass balance models. This reflects the different methods and may also reflect additional mass losses in September captured by GRACE-FO.

The melting and ablation seasons in Greenland began late in 2022 and the summer was relatively cool compared with recent years. However, there was a period of high temperatures at the end of July 2022 with intense melt over large parts of the ice sheet. September 2022 was also extraordinarily warm, with anomalous melting throughout the month (Figure 16). Summit Station, the highest point in Greenland (at an altitude of 3 200 m), had its warmest September on record (since 1991) and experienced melting conditions on 3 September 2022, the first time melting has been registered at this site in September.[38] Later in September, heavy rain associated with post-tropical cyclone *Fiona* fell on the ice sheet, also a first for September. The September mass loss is not included in the –85 Gt cited above, as the end of the Greenland melt season is conventionally taken to be 31 August.

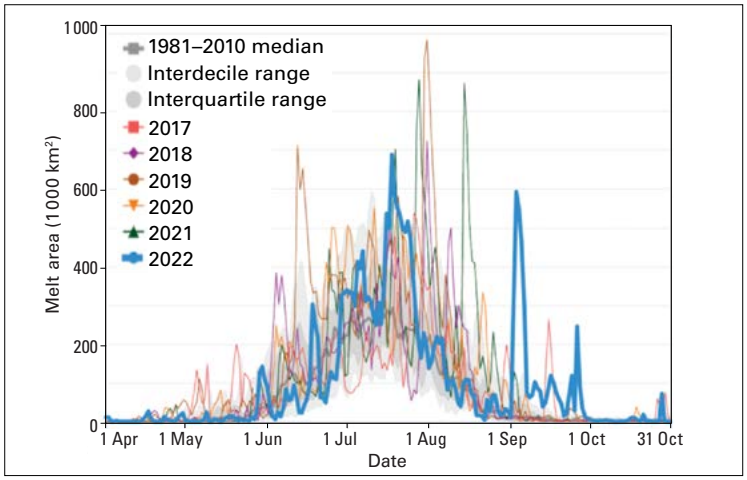

Figure 16. Greenland ice sheet melt area through the 2022 melt season.

Source: Courtesy of NSIDC. Image and analysis courtesy of Thomas Mote, University of Georgia.

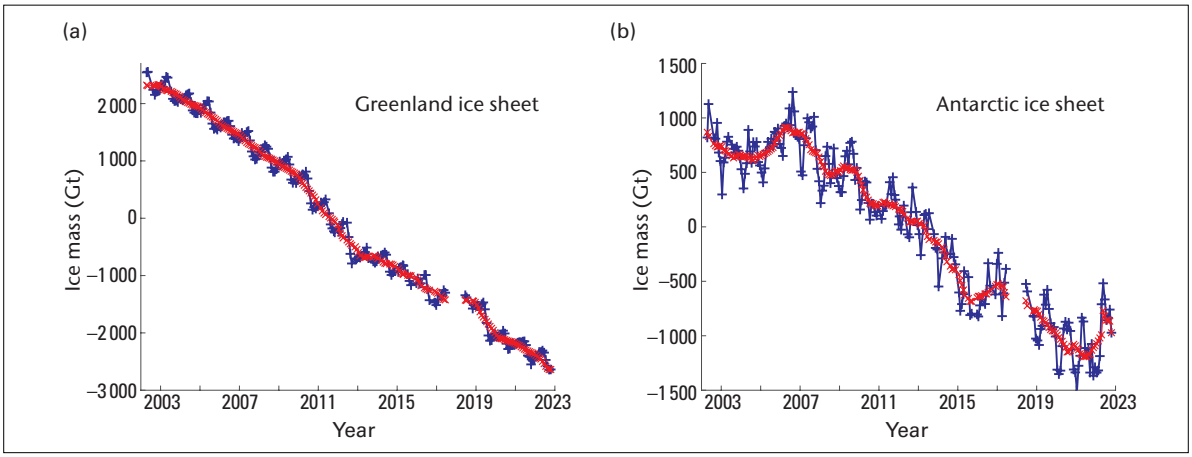

Figure 17. (a) Greenland and (b) Antarctic ice sheet mass balance records from the NASA GRACE and GRACE-FO missions, 2002–2022. Native GRACE data (roughly monthly) are shown in blue, and the red symbols plot the 13-month running mean, which smooths out the seasonal cycle and some of the noise in the signal, better representing the annual mass balance.

Source: Data and analysis courtesy of Isabella Velicogna, University of California, Irvine.

[38] https://nsidc.org/greenland-today/

The Antarctic ice sheet also has a long-term trend of mass loss, with an average rate of mass change of –117 ± 57 Gt per year for the period of record of the GRACE mission, April 2002 to October 2022 (Figure 17(b)). In 2022, the Antarctic ice sheet countered this long-term trend and gained mass, with an estimated mass change of +110 Gt from January to October 2022. Years of positive TMB are not unusual in the GRACE record (see for example 2004, 2005 and 2016), but preliminary results through October 2022 indicate that the ice sheet experienced its greatest mass gain since 2005.

The gain in mass was a result of anomalously high snowfall and SMB (Figure 18). From March 2022 through December 2022, snow accumulation was almost 300 Gt above normal, associated with above-normal temperatures and high snowfall amounts on the western Antarctic Peninsula, Wilkes Land and much of the East Antarctic plateau (Figure 18(c)). The Antarctic ice sheet always has a positive SMB (more snow accumulation than melt), which is countered by marine melt and iceberg discharge. Recent mass losses in Antarctica (Figure 17(b)) of about –100 Gt per year were driven by high rates of marine melting and iceberg discharge on the Amundsen Sea coast. The surplus SMB of about 300 Gt was enough to offset this, leading to a positive TMB in 2022.

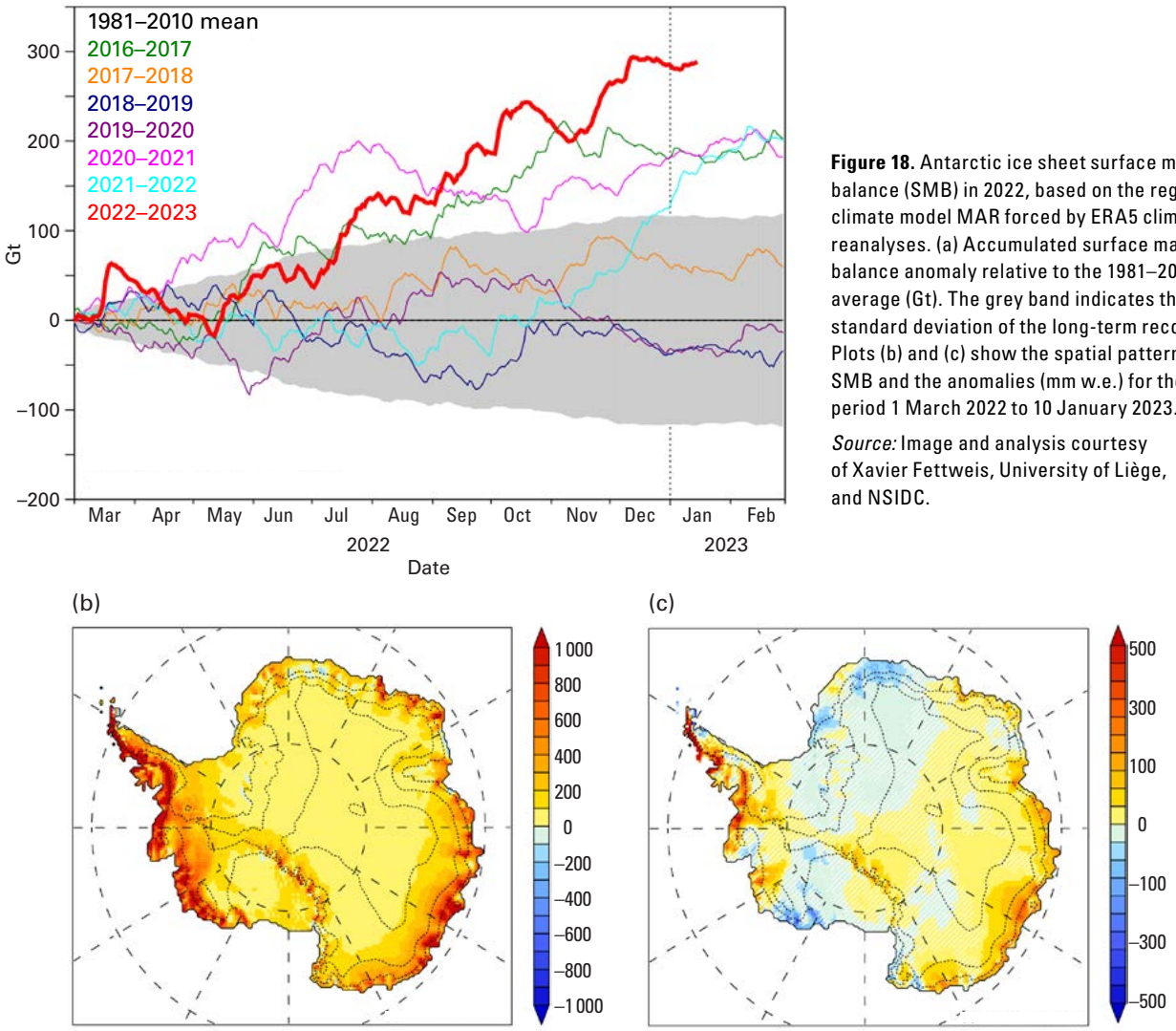

Figure 18. Antarctic ice sheet surface mass balance (SMB) in 2022, based on the regional climate model MAR forced by ERA5 climate reanalyses. (a) Accumulated surface mass balance anomaly relative to the 1981–2010 average (Gt). The grey band indicates the standard deviation of the long-term record. Plots (b) and (c) show the spatial pattern of SMB and the anomalies (mm w.e.) for the period 1 March 2022 to 10 January 2023.

Source: Image and analysis courtesy of Xavier Fettweis, University of Liège, and NSIDC.

SNOW COVER

Seasonal snow cover in the northern hemisphere has been experiencing a long-term decline in the late spring and summer. Snow-cover extent (SCE) in 2022 was close to the 2001–2020 average and was consistent with these long-term trends. Based on analyses of the Rutgers northern hemisphere SCE product,[39] the average daily SCE in the snow season from August 2021 to July 2022 was 2.5% below the 2001–2020 average, with the largest anomalies in June 2022 when snow extent was –1.68 million km^2, 21% below average. Reductions in northern hemisphere spring snow extent are consistent across data sets, and in 2022 the below-average June extent was driven by below-normal snow cover in both North America and Eurasia, where June SCEs were the second and third lowest on record, respectively, for the period 1967–2022.[40]

PERMAFROST

Permafrost is ground (soil and rock) with a temperature that remains below 0 °C for at least two consecutive years. Permafrost can contain significant amounts of ice, and warming and thawing of permafrost can have important implications for landscape stability, hydrology, ecosystems and infrastructure integrity. Frozen soil can also contain carbon which can be released upon thawing, with impacts on GHG concentrations and climate feedbacks. The IPCC AR6 WG I report concluded that "increases in permafrost temperatures in the upper 30 m have been observed since the start of observational programs over the past three to four decades throughout the permafrost regions (*high confidence*)".[41]

Permafrost temperatures are measured in numerous boreholes across the Arctic, with records for some sites now more than four decades long. Temperatures at depths at or near the level of minimal seasonal change indicate that permafrost has been warming since the 1970s (Figure 19), with record high values observed in the most recent available data at

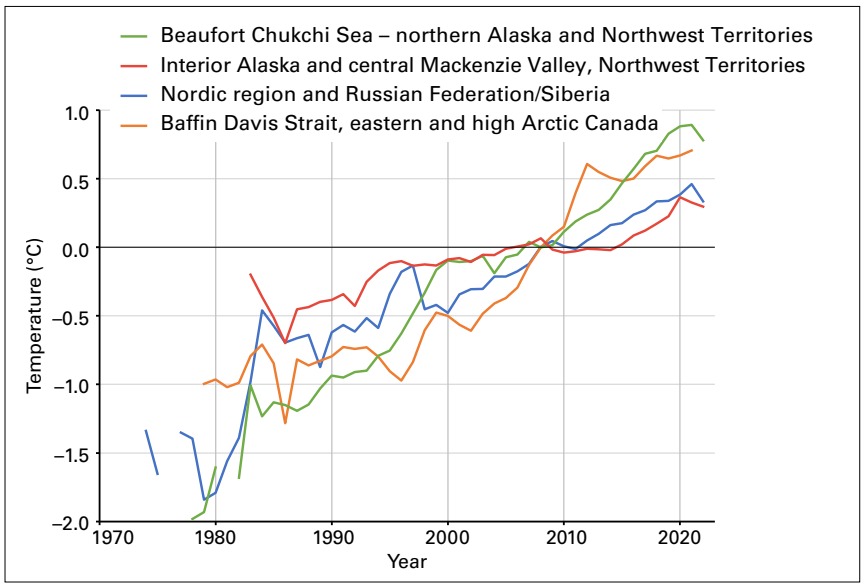

Figure 19. Average departures of permafrost temperature (measured in the upper 20–30 m) 1974–2022 from a baseline established during the International Polar Year (2007–2009) for Arctic regions.

See Smith et al., 2022 (refer to footnote 42) for the location of sites in each region and rates of temperature change for individual sites. Some sites were established after 2000.

[39] https://snowcover.org

[40] Mudryk, L.; Chereque, A. E.; Derksen, C. et al. Terrestrial Snow Cover. In *Arctic Report Card 2022;* Druckenmiller, M. L.; Thoman, R. L.; Moon, T. A., Eds.; National Oceanic and Atmospheric Administration, 2022. https://doi.org/10.25923/yxs5-6c72.

[41] Intergovernmental Panel on Climate Change (IPCC), 2021: Climate Change 2021: The Physical Science Basis, Chapter 2, section 2.3.2.5, Terrestrial Permafrost, https://www.ipcc.ch/report/ar6/wg1/.

many sites.[42] Greater rates of permafrost warming (0.4 °C to 0.6 °C per decade) are generally observed in the colder permafrost (<–2 °C) of the western North American Arctic, the Canadian high Arctic, Nordic regions and Russian Federation/Siberia. In warmer permafrost, with temperatures close to 0 °C, in regions such as interior Alaska and the central Mackenzie valley of Canada, lower rates of warming have been observed (<0.2 °C per decade). The lower rates of temperature increase are due to the phase change as ground ice melts. Although temperatures may change little over time as permafrost temperatures approach 0 °C, the melting of ground ice has important impacts on soil strength and ground stability.

Active layer thickness (ALT) is the maximum thickness of the surface layer that thaws seasonally. The depth of the active layer is increasing worldwide. Of all Arctic regions, the Beaufort Chukchi Sea region has the lowest trend, with an increase of <0.3 cm per year from 2000 to 2021. The situation in interior Alaska and Canada is very different, with ALT increasing by 0.9 cm per year. Thaw depths were substantially greater than average from 2018 to 2021, and ALT in 2021 was the second highest since 2000 (after 2020). ALT in mountain environments is highly variable. Sites in the European Alps show an increase in ALT (>1 cm per year), while sites in the Norwegian Alps have negligible trends. Antarctica has few active sites and the available data suggest relatively small changes, but ALT on the Antarctic Peninsula has increased since 2013.

STRATOSPHERIC OZONE AND OZONE-DEPLETING GASES

Following the success of the Montreal Protocol, production and consumption of halons and chlorofluorocarbons (CFCs) has been reported as discontinued, but their levels in the atmosphere continue to be monitored. Because CFCs have long lifetimes, they will remain in the atmosphere for many decades, and even if there were no new emissions, there would still be more than enough chlorine and bromine present to cause nearly complete depletion of ozone in the lower stratosphere over Antarctica from August to December. As a result, the Antarctic ozone "hole" continues to form every spring, with its area and depth governed to a large degree by meteorological conditions. The "hole" is not strictly a hole; it is an area where the total column ozone in the stratosphere falls below 220 Dobson units.

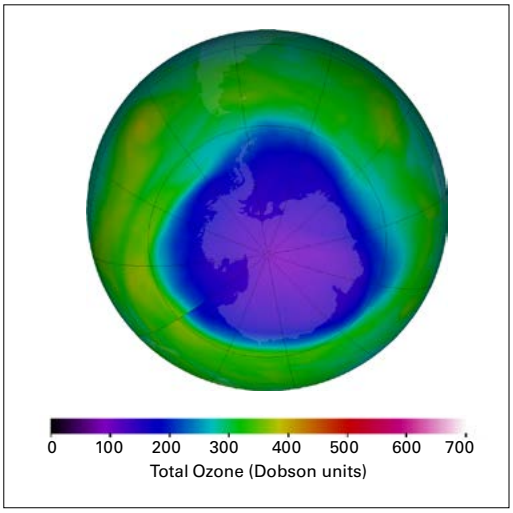

False-colour view of total ozone over the Antarctic pole on 1 October 2022. Purple and blue colours indicate the regions where there is the least ozone, and yellows and reds show where there is more ozone. A movie showing ozone evolution over the full year 2022 is available at: https://ozonewatch.gsfc.nasa.gov/ozone_maps/movies/OZONE_D2022-07-01%25P1D_G%5e360X240.IOMPS_PNPP_V21_MMERRA2_LSH.mp4.

[42] Smith, S. L.; O'Neill, H. B.; Isaksen, K. et al. The Changing Thermal State of Permafrost. *Nature Reviews Earth and Environment* **2022** *3*, 10–23. https://doi.org/10.1038/s43017-021-00240-1.

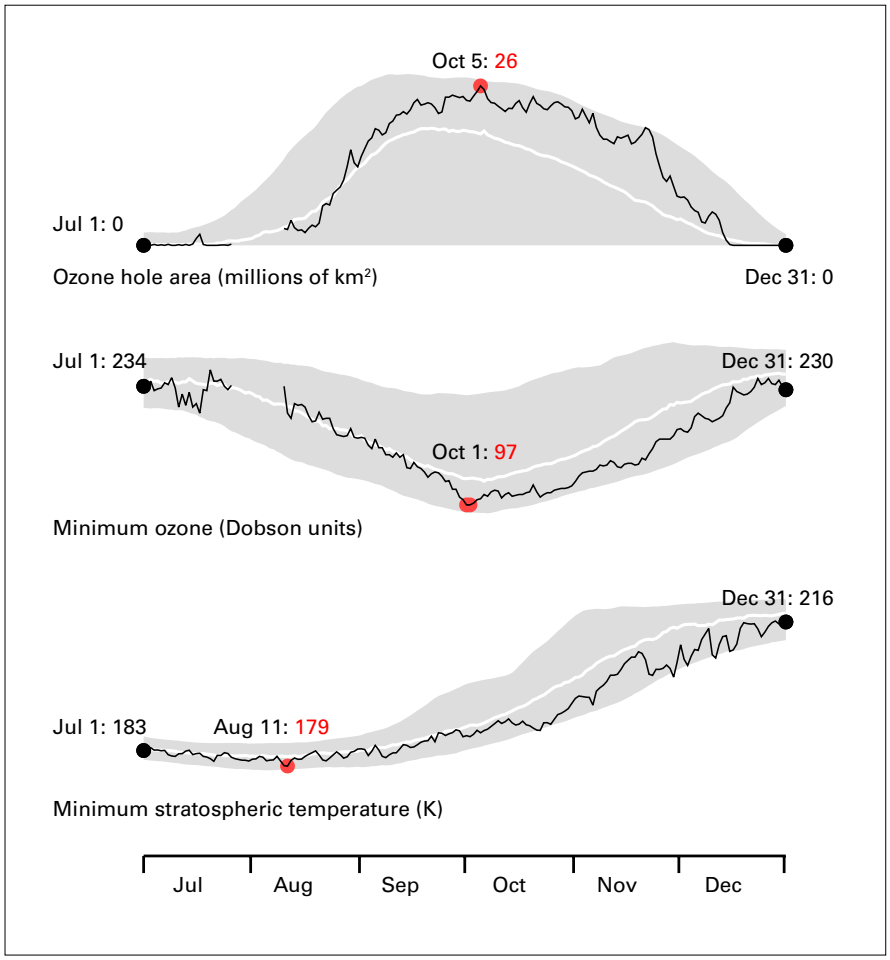

Figure 20. Top: Ozone hole area (millions of square kilometres). Middle: Minimum ozone (Dobson units). Bottom: Minimum stratospheric temperature (K) at the 50 hPa level (~20 km altitude) from 1 July to 31 December 2022. Red numbers give the highest (ozone hole area) or lowest (minimum ozone, minimum stratospheric temperature) value of the season for each indicator.

Source: NASA Ozone Watch.

The evolution of the ozone "hole" in 2022 was similar to its evolution in 2021. The hole developed relatively early and continued growing, resulting in a large and deep ozone hole. On 5 October it reached 26 million km², comparable to 2020 and 2021, and close to the maximum area observed in earlier years such as 2015 (28.2 million km²) and 2006 (29.6 million km²)[43] (Figure 20). NASA reported a minimum ozone column of 97 Dobson units on 1 and 2 October 2022. Concentrations of stratospheric ozone were persistently reduced to near zero between 15 and 20 km altitude over Antarctica at the end of September 2022, which, along with the values measured in the season of 2021, are among the lowest ozone values ever measured via sondes at the Antarctic stations.[44] The unusually deep and large ozone hole was driven by a strong, stable polar vortex and lower-than-average temperatures in the stratosphere.

PRECIPITATION

Precipitation totals were above the long-term (1951–2000) average in North-east Asia, the western Indian summer monsoon region, South-east Asia, the Maritime Continent, areas of Northern South America, parts of North America and the Caribbean, the eastern Sahel region,

[43] https://ozonewatch.gsfc.nasa.gov/

[44] As reported by the National Oceanic and Atmospheric Administration (NOAA).

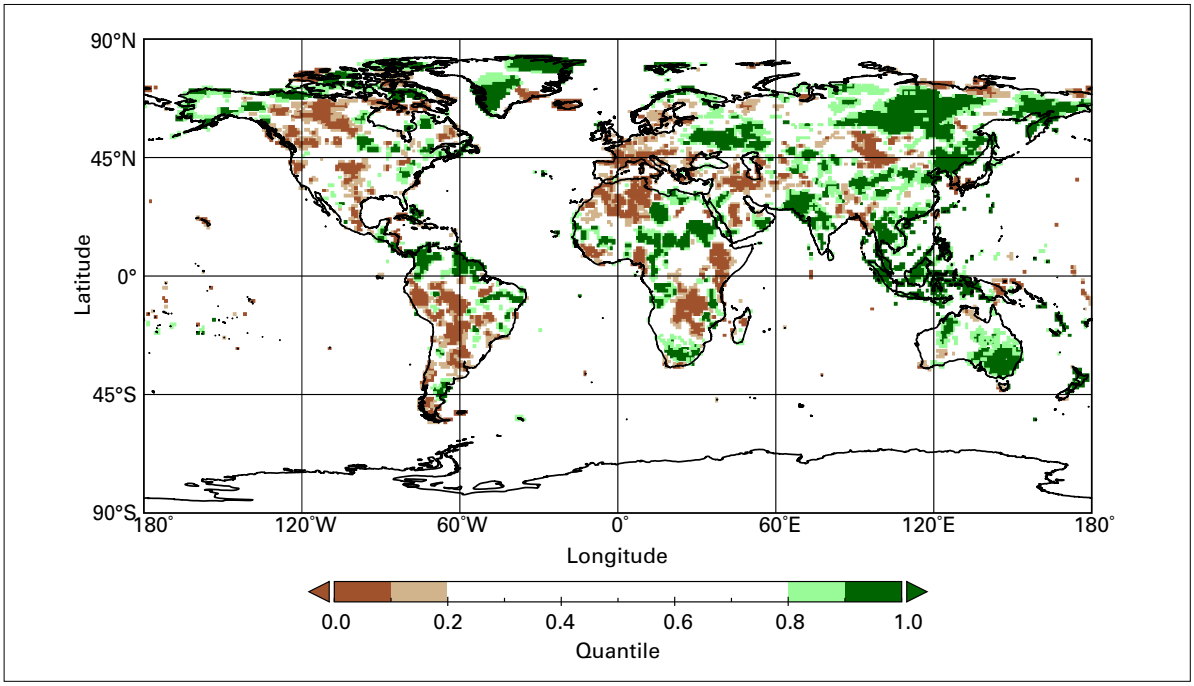

Figure 21. Total precipitation in 2022, expressed as a percentile of the 1951–2000 reference period, for areas that would have been in the driest 20% (brown) and wettest 20% (green) of years during the reference period, with darker shades of brown and green indicating the driest and wettest 10%, respectively.

Source: Global Precipitation Climatology Centre (GPCC), Deutscher Wetterdienst, Germany.

parts of Southern Africa, Sudan, Eastern Europe, New Zealand and Australia (Figure 21). Regions with a marked rainfall deficit included: large parts of Europe, the Mediterranean region and North-west Africa as well as parts of the Middle East; Central Asia and the Himalayas; Eastern Africa and Madagascar; Central and Southern South America; and Central and Western North America (Figure 21).

The Indian Monsoon onset was earlier and the withdrawal later than normal in 2022. The majority of the Indian subcontinent was wetter than average and the monsoon extended farther westward than usual towards Pakistan, where there was extensive flooding. The onset of the West African Monsoon was delayed as it was in 2021. Later in the West African Monsoon season, rainfall totals were higher than normal. In total, the seasonal rainfall was close to normal except in the eastern and western coastal regions.

SHORT-TERM CLIMATE DRIVERS

Climate modes are recurrent patterns, usually of pressure or sea-surface temperature (SST), typically characterized by negative and positive phases, which each have distinctive effects on the distribution of rainfall, temperature and other meteorological elements on time scales varying from days to seasons and beyond.

In 2022, two such climate modes – the El Niño–Southern Oscillation (ENSO) and the Indian Ocean Dipole (IOD) – contributed to major weather and climate events across large areas of the world. Examples are provided in the following sections.

EL NIÑO–SOUTHERN OSCILLATION

ENSO is one of the most important drivers of year-to-year variability in weather patterns worldwide. It is linked to hydrometeorological hazards such as heavy rains, floods and drought. El Niño, characterized by higher-than-average SSTs in the eastern tropical Pacific and a weakening of the trade winds in the region, typically has a warming influence on global temperatures. La Niña, which is characterized by below-average SSTs in the central and eastern tropical Pacific and a strengthening of the trade winds, has the opposite effect.

La Niña conditions emerged in mid-2020 and continued into 2021, with SSTs briefly becoming ENSO-neutral (within 0.5 °C of normal), although still cooler than average during most of the northern hemisphere summer. SSTs decreased again, and La Niña re-emerged during the July–September period of 2021, quickly evolving to moderate strength, where it remained through the end of 2022 (Figure 22). This marks the third consecutive year of La Niña,[45] the third time such an event, informally referred to as a "triple-dip" La Niña, has occurred in the last 50 years, following 1973–1976 and 1998–2001.

As well as having a temporary cooling influence on global mean temperature, La Niña is often – though not always – associated with characteristic patterns of rainfall. In some regions the pattern of precipitation anomalies in 2022 was typical of La Niña: drier than usual conditions in Patagonia and South-west North America, and wetter than usual in Southern Africa, Northern South America, the maritime continent and eastern Australia. In early December, a week-long heatwave with dry conditions and record-breaking maximum temperatures affected Argentina, which is in its third consecutive year of drought. Parts of southern and central Chile, meanwhile, continue to experience drought conditions which have now persisted for more than a decade.[46] La Niña is also associated with more intense and longer monsoon rainfall in South-east Asia. Pakistan experienced record rains in July and August. La Niña and the

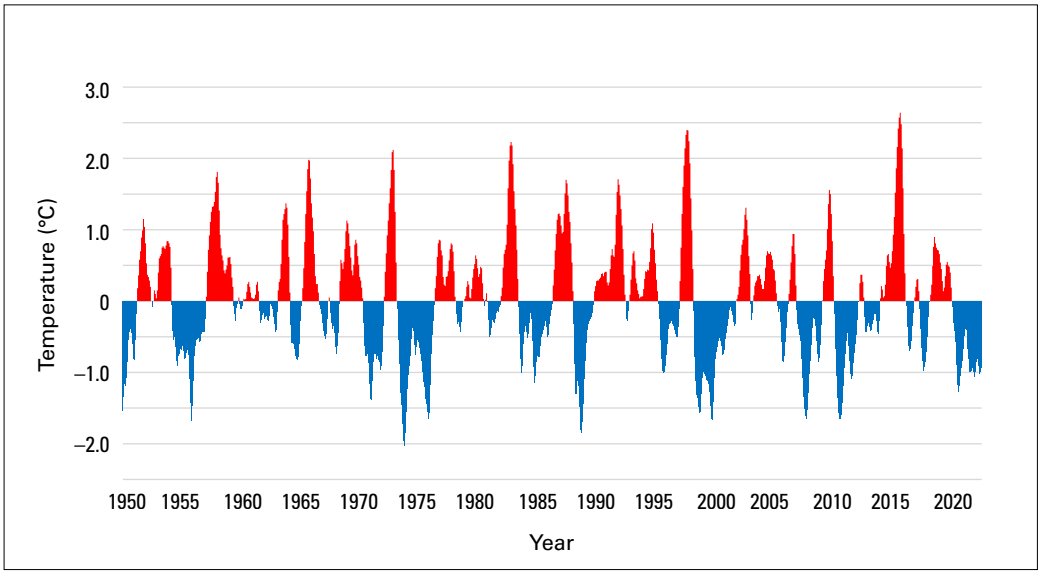

Figure 22. Time series of NOAA's Oceanic Niño index from 1950 to December 2022 showing the presence of below-average conditions (blue) and above average conditions (red) during three-month average time periods.

Source: NOAA, National Centers for Environmental Information (NOAA NCEI).

[45] https://public.wmo.int/en/our-mandate/climate/el-ni%C3%B1ola-ni%C3%B1a-update

[46] Garreaud, R. D.; Alvarez-Garreton, C.; Barichivich, J. et al. The 2010–2015 Megadrought in Central Chile: Impacts on Regional Hydroclimate and Vegetation. *Hydrology and Earth System Sciences* **2017**, *21*, 6307–6327. https://doi.org/10.5194/hess-21-6307-2017.

negative phase of the IOD are associated with drier-than-normal conditions in East Africa.[47] Most of Kenya, Ethiopia and Somalia have experienced five consecutive below-average rainfall seasons, with severe humanitarian impacts.

Although it typically reduces global temperature, La Niña is not associated with lower temperatures everywhere. In New Zealand it is typically associated with warm, wet air masses. The country reported its warmest and wettest winter on record, the third consecutive winter to break the seasonal temperature record, and 2022 was the warmest year on record for the country, surpassing the record set in 2021 by 0.20 °C.

INDIAN OCEAN DIPOLE

The positive phase of the IOD is characterized by below-average SSTs in the Eastern Indian Ocean and above average SSTs in the west. The negative phase has the opposite pattern. The resulting change in the gradient of SST across the ocean basin affects the weather of the surrounding continents, primarily in the southern hemisphere. Positive IOD events are often, but not always, associated with El Niño and negative events with La Niña.

For the second consecutive year, a negative IOD developed during austral winter. In combination with La Niña, this phase contributed to wet conditions across much of Australia in late austral winter and spring. It was the wettest spring and wettest October on record for New South Wales and Victoria, and the second-wettest spring nationally after 2010. Major flooding affected multiple regions in the spring, particularly across large areas of eastern Australia. The negative IOD returned to neutral as austral summer began.

As previously mentioned, the negative IOD, in combination with La Niña, contributed to the ongoing dry conditions in Eastern Africa. More details are to be found in the sections on Extreme events and Socioeconomic impacts.

[47] See e.g. Anderson, W.; Cook, B. I.; Slinski, K. et al. Multiyear La Niña Events and Multiseason Drought in the Horn of Africa, *Journal of Hydrometeorology* **2023**, *24* (1), 119–131. https://doi.org/10.1175/JHM-D-22-0043.1.

Extreme events

Although broad-scale changes in the climate are important, the impacts of weather and climate are most clearly felt during extreme events such as heavy rain and snow, droughts, heatwaves, cold spells and storms, including tropical storms and cyclones. These meteorological and climatological extremes, individually, in combination and in conjunction with other factors, can lead to other events such as flooding, landslides, wildfires and compound extremes. Together, these have a wide range of impacts on human and natural systems. This section, which describes a selection of extreme events in 2022, is based largely on input from WMO Members. The wider socioeconomic risks and impacts are described in the section on Socioeconomic impacts. Additional information comes from EM-DAT.[48]

HEAT, DROUGHT AND WILDFIRES

China had the most extensive and long-lasting heatwave since national records began, extending from mid-June to the end of August and resulting in the hottest summer on record by a margin of more than 0.5 °C. It was also the second-driest summer on record, with most of the southern half of China (apart from Guangdong province) having seasonal rainfall 20% to 50% below average. Across the country 366 locations had their highest temperature on record. The heat was particularly severe in the Yangtze River valley, which also suffered from significant drought during its driest summer on record; the Yangtze River at Wuhan reached the lowest level ever recorded for August. There were also numerous wildfires in the region. There were significant heatwaves elsewhere in East Asia, including a record nine consecutive days above 35 °C in Tokyo from 25 June to 3 July 2022.

Europe also experienced numerous heatwaves, with significant heatwaves occurring in each of the three summer months. During the summer, around 4 600 deaths in Spain, 4 500 in Germany,[49] 2 800 in the United Kingdom[50] (among those aged 65 and older), 2 800 in France[51] and 1 000 in Portugal were associated with the unusual heat. The most exceptional heatwave occurred in mid-July. Temperatures reached 40 °C in the United Kingdom for the first time (Figure 23), with a reading of 40.3 °C at Coningsby on 19 July,[52] while 33.0 °C on 18 July at Phoenix Park (Dublin) was the highest in Ireland since 1887. Numerous locations broke previous records by more than 3 °C, particularly in northern England and western France. A temperature

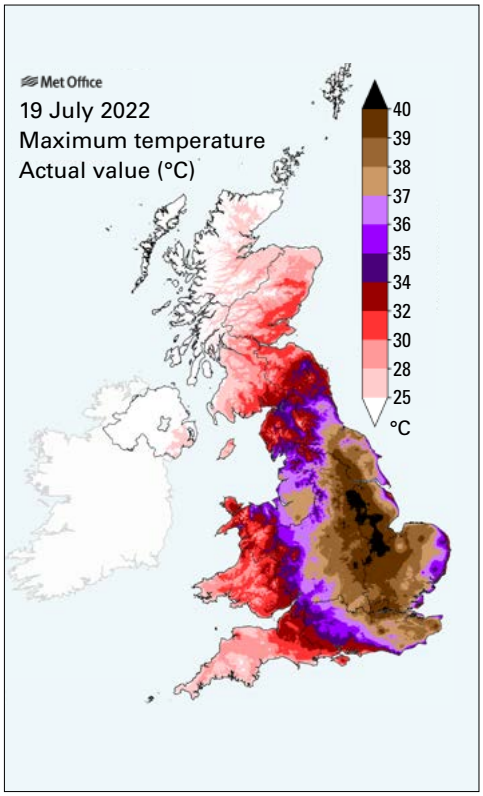

Figure 23. United Kingdom maximum temperatures for 19 July.

Source: Met Office, United Kingdom.

[48] https://www.emdat.be/

[49] https://www.rki.de/DE/Content/Infekt/EpidBull/Archiv/2022/42/Art_01.html

[50] https://www.ons.gov.uk/peoplepopulationandcommunity/birthsdeathsandmarriages/deaths/articles/excessmortalityduringheatperiods/englandandwales1juneto31august2022

[51] https://www.santepubliquefrance.fr/presse/2022/bilan-canicule-et-sante-un-ete-marque-par-des-phenomenes-climatiques-multiples-et-un-impact-sanitaire-important

[52] https://www.metoffice.gov.uk/about-us/press-office/news/weather-and-climate/2022/july-heat-review

of 40.1 °C at Hamburg-Neuwiedenthal on 20 July was the northernmost 40 °C reading on record in Germany. The heat extended as far north as Sweden, where the reading of 37.2 °C at Målilla on 21 July was the country's highest since 1947.

The Mediterranean region experienced major heatwaves in June and August. A number of June record high temperatures were set in Italy, including 40.0 °C at Urbe (Rome) on 27 June. Tunisia had its hottest June on record, and some locations set all-time record highs in August, while a record high of 49.1 °C was set at Smara (Morocco) on 10 July. North-east Europe had major heatwaves in mid-August with records set in Finland and Estonia. Nearly the entire Mediterranean Sea was affected by marine heat waves, which lasted from March to December, setting new records for cumulative intensity in the region.

Drought also affected many parts of Europe and the Mediterranean (Figure 24). In Europe, conditions were at their most severe in August, when rivers including the Rhine, Loire and

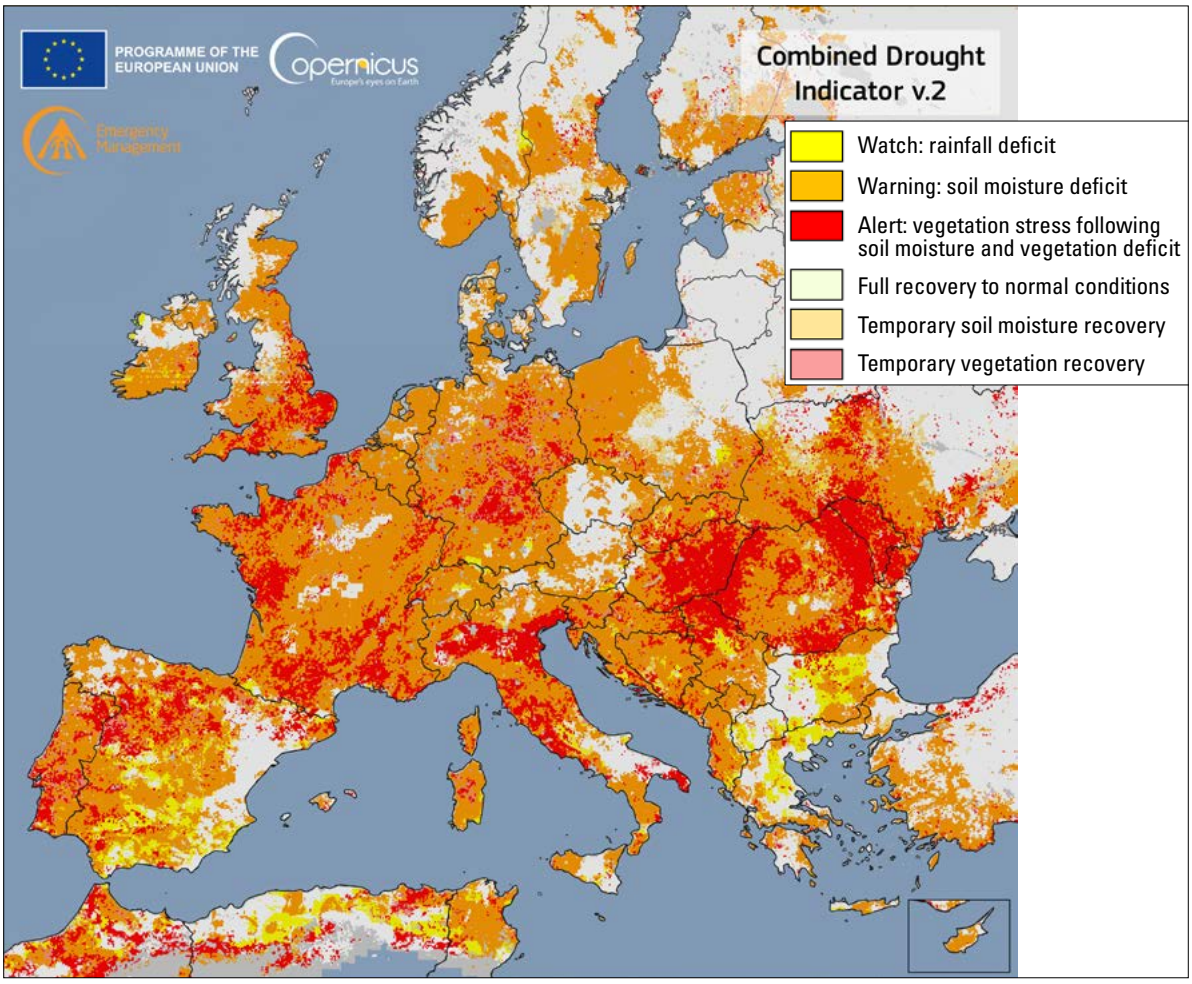

Figure 24. European drought – Copernicus Emergency Management Service Combined Drought Indicator for 1–10 August 2022. Yellow areas are under a "watch" state indicating a rainfall deficit, orange areas are under a "warning" state indicating a soil moisture deficit and red areas are under an "alert" state indicating vegetation stress following soil moisture and rainfall deficits.

Source: https://edo.jrc.ec.europa.eu/documents/news/GDO-EDODroughtNews202208_Europe.pdf, CC-BY 4.0 licence.

Danube fell to critically low levels, significantly disrupting river transport. In France, low river flows, and high river-water temperatures led to output being reduced at some nuclear power stations.[53] Three states in west-central Germany had their driest summer on record, in a region which had experienced extreme flooding the previous summer. France had its driest January to September period since 1976, and the United Kingdom and Uccle (Belgium) had their driest January to August since 1976, while the 12 months ending in August 2022 were the driest for at least 40 years in Morocco. Northern Italy and the Iberian Peninsula were exceptionally dry in winter 2021/2022, and spring was drier than average across large areas of Europe. Significant drought also continues to affect parts of South-west Asia, particularly the Islamic Republic of Iran and Iraq. Baghdad had 24.3 mm of rainfall from September 2021 to May 2022, 78% below the long-term average.

South-western France was severely affected by wildfires, with over 62 000 ha burnt. For the second consecutive year, wildfires were associated with major loss of life in Algeria, with 44 deaths reported from 16 to 18 August.

The pre-monsoon period was exceptionally hot in India and Pakistan. Pakistan had its hottest March and hottest April on record, with both months having national mean temperatures more than 4 °C above the long-term average. In India, grain yields were reduced by the extreme heat and there were a number of forest fires, particularly in Uttarakhand.

Drought intensified in the Greater Horn of Africa region, focused on Kenya, Somalia and southern Ethiopia. Rainfall was well below average across the region in the March–May and October–December rainy seasons, the fourth and fifth consecutive poor wet seasons since the second half of 2020, the longest such sequence in 40 years, with major impacts on agriculture and food security. As in the previous prolonged drought in 2010–2012, La Niña and the negative IOD were substantial contributors to the dry conditions. Significant rain fell during 2021–2022 in many parts of Southern Africa, with some easing of the long-term drought which has been affecting southern Madagascar.

The first half of January was extremely hot in many parts of subtropical South America. The temperature of 44.0 °C recorded at Paysandú on 14 January equalled Uruguay's national record. There were also extensive and prolonged wildfires in northern Argentina and Paraguay, with over 900 000 hectares burned in Corrientes province between early January and late February.[54] Significant drought continued in many parts of the region. Although 2022 rainfall in Chile was not as far below average as in recent years, it was still well below average in places.[55] Buenos Aires had its first rainless June on record, and much of north-eastern Argentina from the Buenos Aires region northwards was in severe drought by the end of the year. For this region, as well as for Uruguay, it was the third consecutive year of significantly below-average rainfall. After a cool autumn and winter, extreme heat returned to the region late in the year with heatwaves in November and December, including a December record high temperature of 46.0 °C on 7 December at Rivadavia (Argentina). Fire activity in the Brazilian Amazon was near the 1998–2021 average, but also among the highest of the last decade.[56] Estimated wildfire carbon emissions in Amazonas state were the highest in at least 20 years.[57]

---

[53] 2022 State of Climate Services: Energy (WMO-No. 1301).

[54] https://twitter.com/INTARNaturales/status/1497310851052630016

[55] Garreaud, R. D.; Boisier, J. P.; Rondanelli, R. et al. The Central Chile Mega Drought (2010–2018): A Climate Dynamics Perspective. *International Journal of Climatology* **2020**, *40*, 421–439. https://doi.org/10.1002/joc.6219.

[56] https://queimadas.dgi.inpe.br/queimadas/aq1km/

[57] https://atmosphere.copernicus.eu/wildfires-amazonas-records-highest-emissions-20-years

Significant drought continued in much of the western half of North America. In the United States, drought conditions covered many western and southern states, although summer monsoon rains brought some relief to the interior south-west, and rains late in the year resulted in some easing of drought in California and the lower Mississippi valley. Total economic losses during the year from drought were assessed at US$22 billion. Texas, which had its second-driest January to July on record, and adjacent areas of northern Mexico were especially dry, while California had its driest January to October on record (65% below the 1901–2000 average), continuing a long-term drought in which precipitation for the 36 months ending October 2022 was the lowest on record. In late July, Lake Mead in the Colorado River basin reached its lowest level since the reservoir was filled in 1938. Drought extended to many other parts of the southern United States during the year. River levels reached record lows during October in places on the middle and lower Mississippi, and more than 82% of the contiguous United States was experiencing abnormally dry conditions by mid-October, the largest such area in the 23-year history of the U.S. Drought Monitor. Heavy spring precipitation eased drought in the north-central United States and the Prairie Provinces of Canada.

Total area burned during the United States wildfire season was slightly above average, with one of the most active seasons on record in Alaska and the largest recorded fire in New Mexico, but loss of life and property was lower than in most recent years. The July to September period was the hottest on record for many parts of the western United States.

Exceptionally high regional temperatures occurred over the plateau of East Antarctica in mid-March as an atmospheric river originating near Australia brought warm, moist air over the Antarctic continent. On 18 March, temperatures reached –10.1 °C at Dome C and –17.7 °C at Vostok. Both values were more than 15 °C above previous March records at the sites and 35 °C above March averages, with the Dome C reading being the highest on record at any time of year.

COLD EXTREMES

Few significant cold records were set globally in 2022. In late December, an intense cold outbreak affected many parts of the United States and Canada. Intense blizzards affected Buffalo and surrounding areas, with significant loss of life. Blizzard conditions lasted 36 hours, with a storm total snowfall of 132 cm. Further west, Casper (Wyoming) had its lowest temperature on record (–41.1 °C). December was also cold in parts of Europe, particularly in the north and north-west. A maximum of –9.3 °C at Braemar on 12 December was the lowest maximum temperature in the United Kingdom since December 2010, while Iceland had its coldest December since 1973.

Greece had two significant snow events in late January and mid-March. Both cold outbreaks also affected other parts of the eastern Mediterranean, with snow falling at elevations above 600 m in Libya. For the second consecutive year, widespread frosts in early April resulted in crop losses in Western Europe, particularly in France. A coastal low brought Boston in the United States 60 cm of snowfall on 29 January, equalling the daily record. It was a snowy winter in Argentine Patagonia; northern Patagonia had its second-most extensive snow cover in the twenty-first century and southern Patagonia its third-most. A cold spell in July brought Puerto Natales (Chile) its second-coldest temperature on record, –16.2 °C, with El Calafate (Argentina) reaching –16.5 °C.

FLOODING AND HEAVY RAIN

Pakistan experienced exceptional flooding (Figure 25) during the monsoon season, peaking in late August. July (181% above normal) and August (243% above normal) were each the wettest on record nationally. Sindh province was particularly badly affected, with Balochistan also hard-hit. Preliminary satellite data indicated that 75 000 km^2, about 9% of Pakistan's area, were inundated at some stage during August.[58] Adjacent areas of Afghanistan were also affected. Over 1 700 deaths were reported in Pakistan and over 2 million dwellings damaged or destroyed, with over 33 million people affected in some way.[59] Crop and livestock losses were also severe, as the floods affected much of the country's agricultural land. Total damage

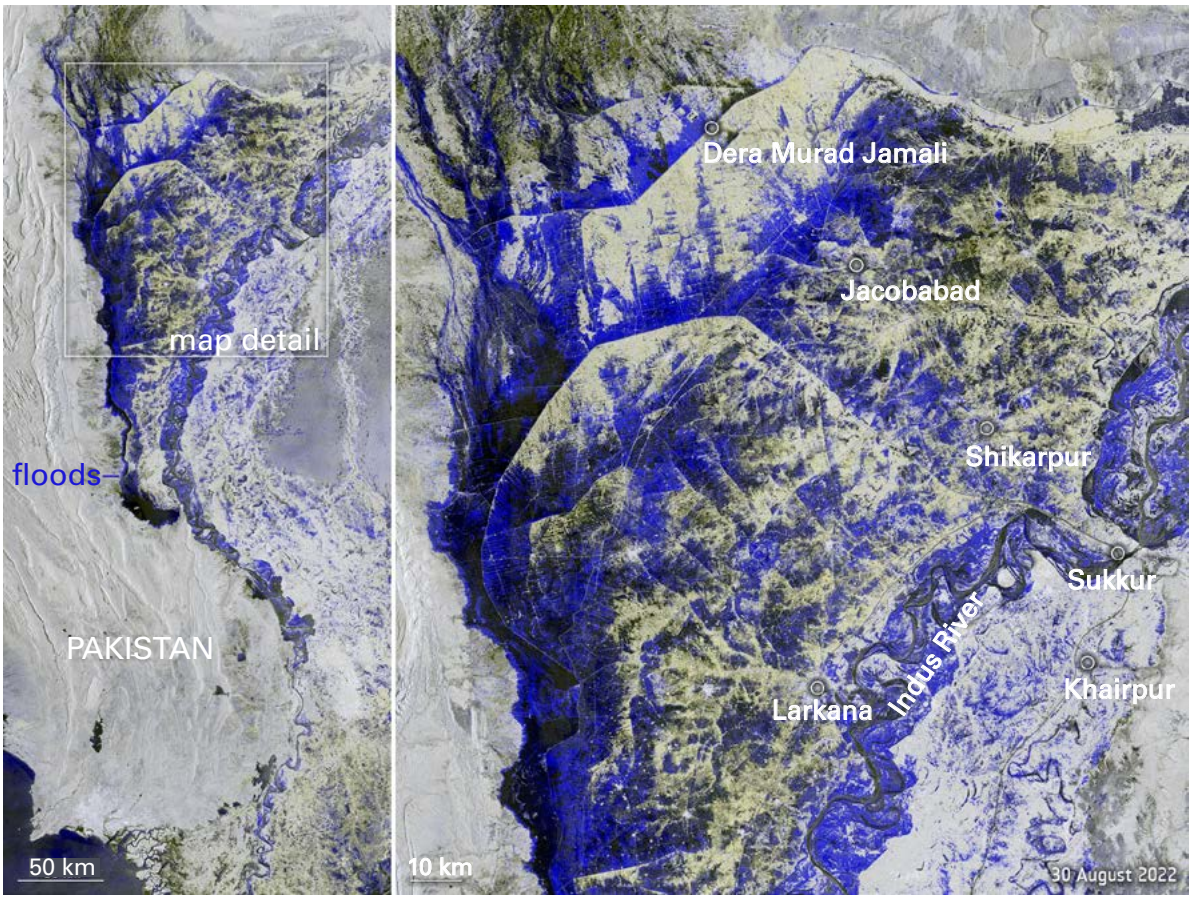

Figure 25. Satellite image of flooding in Pakistan on 30 August. The left side of the image shows a wide view of the area affected and the right side shows an enlarged view of the area between Dera Murad Jamali and Larkana. The blue to black colours show where the land is submerged.

Source: Image from Copernicus Sentinel-1. Contains modified Copernicus Sentinel data (2022), processed by ESA, CC BY-SA 3.0 IGO (https://www.esa.int/ESA_Multimedia/Images/2022/09/Pakistan_inundated).

[58] https://www.unitar.org/maps/map/3604

[59] https://reliefweb.int/report/pakistan/ndma-monsoon-2022-daily-situation-report-no-115-dated-6th-oct-2022
https://reliefweb.int/report/pakistan/ndma-monsoon-2022-daily-situation-report-no-129-dated-20th-oct-2022

and economic losses were assessed at US$ 30 billion.[60] The impacts of the floods were broadly similar to those of 2010. There was also significant flooding in India at various stages during the monsoon season, particularly in the north-east in June, with over 700 deaths reported during the season from flooding and landslides, and a further 900 from lightning.

There was flooding in eastern Australia on numerous occasions during the year. The most severe floods were in late February and early March, affecting eastern coastal areas in south-east Queensland, northern New South Wales and the area around Sydney. The worst flooding was south of Brisbane, where the Wilsons River exceeded previous record levels by about 2 m. In western Sydney the Hawkesbury-Nepean Rivers reached their highest level since 1978. Twenty-two deaths were reported and insured losses were near US$ 4 billion. The Sydney region also had major flooding in early July. There was further major flooding in many parts of the south-east quarter of Australia in the final quarter of the year, particularly in the rivers of the Murray-Darling basin. New South Wales and Victoria both had their wettest spring on record. Flooding continued into early 2023 in the lower Murray-Darling basin as water drained slowly downstream, with some parts of the Murray River in South Australia reaching their highest peak since 1956. Sydney received 2530 mm of rain for the year, well above its previous full-year record of 2194 mm.

The eastern Brazilian city of Petropolis experienced extreme rainfall and flash flooding twice in the space of a few weeks, on 15 February and 20 March. In the February event 250 mm of rain fell in three hours, while in March 415 mm fell in 10 hours. Two hundred and thirty deaths were reported in the February event, many of them as a result of landslides. North-east Brazil also had significant flooding in May, while later in the year, flooding affected many parts of Venezuela after heavy rains in October and November. In the worst single incident, 50 deaths were reported with 56 people missing after a landslide in Tejerìas on 8 October 2022.

Many parts of the Sahel, particularly its eastern half, saw significant flooding during the monsoon season, especially towards its end. Nigeria, Niger, Chad and the southern half of Sudan were particularly affected. The flooding was exacerbated in Nigeria when heavy local rains in October fell as floodwaters arrived from upstream. Over the course of the season, 603 deaths in Nigeria and 159 in Niger were attributed to flooding, with US$ 4.2 billion in reported economic losses in Nigeria. Over 250 000 people were displaced in Chad's capital, N'Djamena, between October and December.[61] While rainfall in South Sudan, where prolonged flooding occurred in 2020 and 2021, was near or below normal, extensive flooding continued as a result of flows from upstream.

TROPICAL CYCLONES

Tropical cyclone activity was near or below average in most regions in 2022, except for the South Indian Ocean, which had an active season overall despite an unusually late start. The South Indian Ocean had one of the season's highest-impact systems; subtropical depression *Issa*, in combination with a cut-off low-pressure system, caused extreme flooding in April in the KwaZulu-Natal province of eastern South Africa, with rainfall totals of up to 311 mm in 24 hours on 11–12 April. Over 400 deaths were attributed to the flooding[62] and 40 000 people

[60] https://www.undp.org/sites/g/files/zskgke326/files/2022-12/Pakistan%20PDNA%20Main%20Report%20-%20Final.pdf

[61] https://www.fmhds.gov.ng/news/flood-fg-begins-delivery-of-12000-metric-tonnes-of-food-items-to-anambra-jigawa-others/

[62] Hendriks, S. L.; Benton, T.; de la Mata, G. C. et al. Global Environmental Climate Change, Covid-19, and Conflict Threaten Food Security and Nutrition. *British Medical Journal* **2022**, *378*, e071534. https://doi.org/10.1136/bmj-2022-071534.

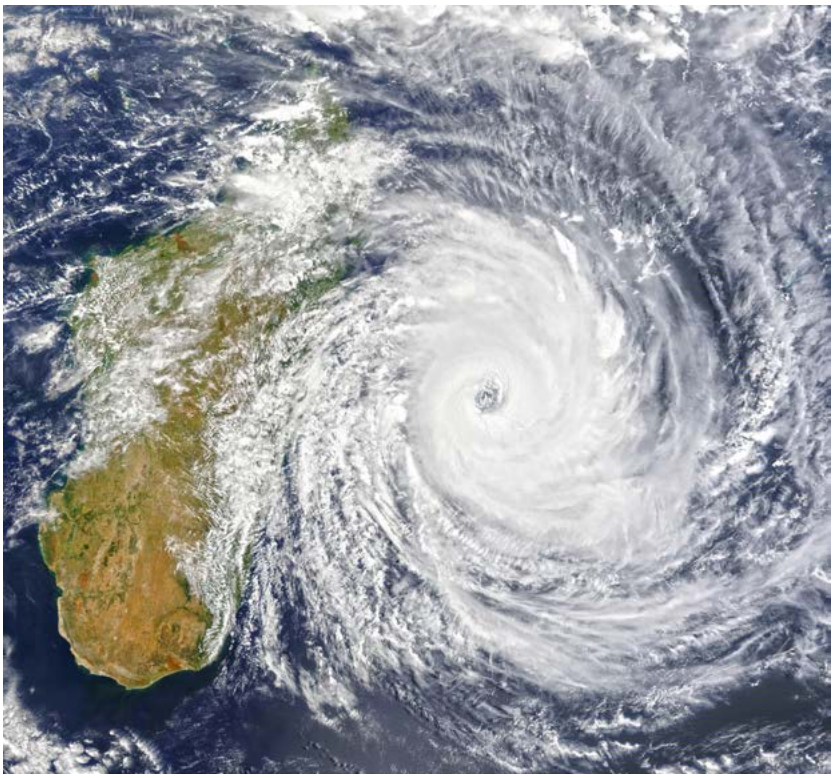

Figure 26. Cyclone *Batsirai*, 4 February 2022, prior to landfall on the east coast of Madagascar.

Source: NASA Earth Observatory, public domain image (https://earthobservatory.nasa.gov/images/149420/bracing-for-batsirai).

were displaced. Madagascar had four landfalls in the space of a month in late January and February. *Ana* (in January) and *Batsirai* (in February, Figure 26) both caused significant loss of life there, with *Ana* also going on to have major impacts from flooding in Mozambique and Malawi. *Gombe* (March) brought flooding to Mozambique with significant casualties.

The North Atlantic hurricane season had an inactive start compared with recent years but had two major landfalls in September. Hurricane *Ian* crossed western Cuba before intensifying to category 4 and making landfall in south-west Florida on 28 September. *Ian* brought extensive storm-surge inundation in low-lying coastal areas and river flooding further north-east, where four-day rainfall exceeded 500 mm around Daytona Beach. Sustained 10-minute winds of 241 km per hour made *Ian* the fourth strongest landfall on record in Florida. Economic losses from *Ian* in the United States were assessed at US$ 113 billion, making it the third most costly tropical cyclone on record, while with 152 deaths, it caused the greatest loss of life in a Florida tropical cyclone since the 1930s.[63,64]

Hurricane *Fiona* crossed the Dominican Republic, Puerto Rico and the Turks and Caicos Islands in September, causing significant flooding and widespread power outages, before intensifying and tracking north towards Canada. It made landfall as a transitioning extratropical storm in Nova Scotia on 24 September with an estimated central pressure of 931 hPa. Hart Island reported 932.7 hPa, the lowest mean sea level pressure on record at a Canadian station. There was widespread wind damage and power outages, and substantial storm surge and wave flooding in coastal areas, particularly in south-western Newfoundland.

[63] https://www.ncei.noaa.gov/access/monitoring/monthly-report/national/202209/supplemental/page-5

[64] https://www.ncei.noaa.gov/access/billions/events/US/2022

The western North Pacific had a below-average season, particularly for intense cyclones, but still had a number of significant impacts. The two most destructive systems were both of tropical storm intensity when they hit the Philippines but nonetheless caused major loss of life through severe flooding and landslides. Tropical Storm *Megi* (*Agaton*) crossed the Philippines on 10–12 April and *Nalgae* (*Paeng*) did so on 29–30 October. Over 200 deaths were attributed to *Megi* and over 150 to *Nalgae,*[65] with *Megi*'s worst impacts being experienced around Cebu, whilst those from *Nalgae* affected many parts of the country. Floods associated with monsoonal rains also resulted in significant loss of life in Mindanao in the last week of December.

The two strongest systems of the season both occurred in September. Typhoon *Hinnamnor* had significant impacts when it reached the Korean Peninsula in early September despite some weakening before landfall, while Typhoon *Nanmadol* affected southern Japan. Also in September, although it had limited impact as a tropical system, after transitioning to an extratropical system and moving north-east, Typhoon *Merbok* caused major coastal inundation in western Alaska.

SEVERE STORMS

An exceptional *derecho*[66] affected parts of southern and central Europe on 18 August, bringing severe winds and heavy rainfall on a track which extended 1600 km from the Balearic Islands (Spain) across Corsica (France), Italy, Slovenia, Austria and Czechia. The system reached its peak severity over Corsica, where wind gusts of 225 km per hour were recorded, the strongest reliably observed wind gust on record for metropolitan France.[67] Five deaths were reported. There was also significant damage in Italy, where hail reached 8 cm in diameter. On 23 October, an EF3 tornado crossed northern France causing significant damage; its path was 206 km long, the longest recorded in France. The most significant windstorm of the western European season was *Eunice*, which crossed England and Wales on 18 February. A gust of 196 km per hour at The Needles (on the Isle of Wight) was the highest on record in England. Four deaths occurred during the storm in the United Kingdom, four in the Kingdom of the Netherlands and a further two in Belgium, while more than a million households in England and Wales lost power.

The United States tornado season had a near-average number of tornadoes, despite a very active March, but casualties were below long-term averages. There were numerous flash flood events during the summer across various parts of the country, including Yellowstone National Park in June, St. Louis and eastern Kentucky in July, Death Valley on 5 August and Dallas-Fort Worth on 22 August. In the Kentucky event, where daily rainfalls were between 100 and 200 mm, at least 37 deaths were reported, while in the Dallas event some locations received more than 300 mm in 12 hours. Flooding of a treatment plant cut the water supply in Jackson (Mississippi) in late August.

Abnormal rainfall and storm activity affected South-west Asia and the Arabian Peninsula in late July and early August, normally a dry time for the region. Fujiarah Port (United Arab Emirates) received 255.2 mm over two days on 27 and 28 July. Flash flooding occurred in many locations and significant casualties were reported in Yemen and Iran. There was further intense rainfall and flash flooding in November; Jeddah (Saudi Arabia) received 179 mm in six hours on 24 November, about three times its average annual rainfall.

---

[65] https://www.typhooncommittee.org/17IWS/docs/Members%20REport/Philippines/2022_IWS%20Member%20Report%20-%20Philippines.pdf

[66] According to the American Meteorological Society, a *derecho* is a "widespread convectively induced straight-line windstorm."

[67] https://meteofrance.fr/sites/meteofrance.fr/files/files/editorial/Bilan%20%C3%A9t%C3%A9%202022%202e%20partie_C.pdf

Socioeconomic impacts

The risks posed by weather and climate-related hazards are complex and context specific, depending on the vulnerability, exposure and adaptive capacity of human and natural systems. Weather and climate-related events pose multiple humanitarian risks to society. Climate and extreme weather events also affect the use and distribution of natural resources across regions and within countries and have large negative impacts on the environment.

In the face of global systemic risk, such as climate change, changes in how society addresses disaster risks are needed.[68] Governments have been making consistent efforts to address disaster and climate risks and build resilience. Around 125 countries have developed national disaster risk reduction strategies (Target E of the Sendai Framework).[69] However, international cooperation and financing for disaster risk reduction remains low.[70] One of the essential components for reducing the impact of disasters is to have effective multi-hazard early warning systems (MHEWSs), and to have people act on the warnings. There is evidence suggesting that countries reporting good MHEWS coverage have lower mortality rates compared to countries that have little or no such coverage.[71] The UN Secretary-General has tasked WMO with leading action to ensure every person on Earth is protected by early warning systems within five years.[72]

FOOD SECURITY

As of 2021, 2.3 billion people faced food insecurity, of whom 924 million faced severe food insecurity. Projections estimated that 767.9 million were people facing undernourishment in 2021, or 9.8% of the global population (Figure 27). Half of the 767.9 million are in Asia and

Figure 27. Percentage of undernourishment (orange, left axis) and number of undernourished people (grey line, right axis) at the global level.

Source: FAO, IFAD, UNICEF, WFP, WHO (2022) (see footnote 73).

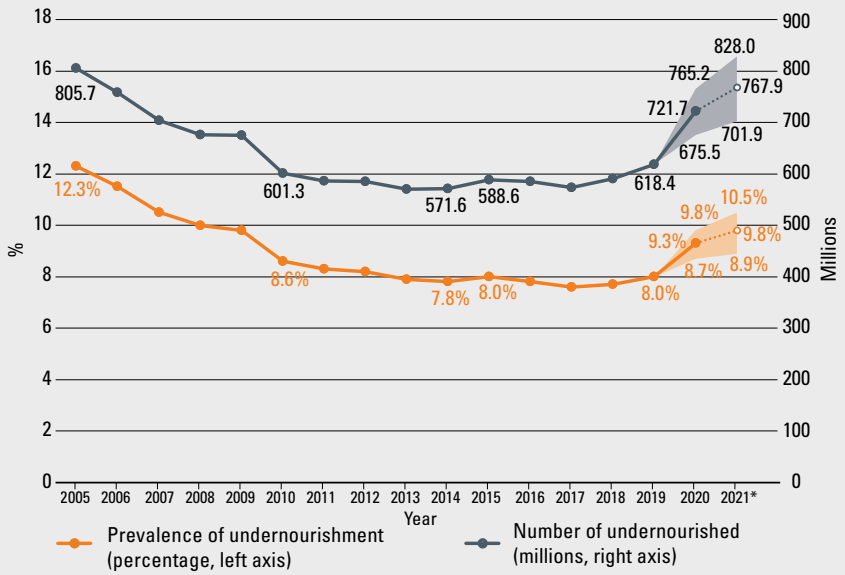

* Projected values for 2021 are illustrated by dotted lines. Shaded areas show lower and upper bounds of the estimated range.

[68] https://www.undrr.org/gar2022-our-world-risk

[69] https://www.undrr.org/publication/global-status-multi-hazard-early-warning-systems-target-g

[70] https://www.undrr.org/publication/international-cooperation-disaster-risk-reduction-target-f

[71] https://www.undrr.org/publication/global-status-multi-hazard-early-warning-systems-target-g

[72] https://public.wmo.int/en/earlywarningsforall

one third are in Africa.[73] Rising undernourishment has been exacerbated by the compounded effects of hydrometeorological hazards and COVID-19 on health, food security, incomes and equality, as well as the effects of protracted conflicts and violence.[74] As of October 2022, several countries in Africa and Asia (such as Ethiopia, Nigeria, South Sudan, Somalia, Yemen, and Afghanistan) and the Caribbean (Haiti) experienced starvation or death and required urgent humanitarian action (IPC Phase 5: *Catastrophe*[75]). In these countries, the key drivers and aggravating factors for acute food insecurity were conflict/insecurity, economic shocks, political instability, displacement, dry conditions and cyclones.

Heatwaves in the 2022 pre-monsoon season in India and Pakistan caused a decline in crop yields. This, combined with the banning of wheat exports and restrictions on rice exports in India after the start of the conflict in Ukraine, has threatened the availability, access to and stability of staple foods within international food markets and posed high risks to countries already affected by shortages of staple foods.[76] Heavy monsoon rains caused severe flooding and landslides in Pakistan, leading to the spread of water-borne diseases, with the greatest impacts in the most vulnerable and food-insecure regions of southern and central Pakistan. Over 1 700 people died,[77] along with 936 000 head of livestock. Large areas of croplands were affected[78] and rainfall-triggered flooding and landslides also substantially disrupted transportation and building infrastructure.[79,80]

Protracted La Niña conditions that persisted from 2020 to early 2023 may have intensified droughts and, consequently, crop and livestock losses in Central Asia much like the protracted 1998–2001 La Niña.[81,82] As of September 2022, food insecurity concerns remained at the highest level for Afghanistan, and around 18.9 million people (45% of the population) were expected to face Level (3) (*Crisis*) or worse levels of acute food insecurity from June to November 2022. In the Syrian Arab Republic, the 2021–2022 season had poor rainfall and dry spells, constraining crop yields for the second consecutive season. The 2022 winter growing

---

[73] Food and Agriculture Organization of the United Nations (FAO), International Fund for Agricultural Development (IFAD), United Nations Children's Fund (UNICEF), World Food Programme (WFP), World Health Organization (WHO), 2022: *The State of Food Security and Nutrition in the World 2022: Repurposing Food and Agricultural Policies to Make Healthy Diets More Affordable*, https://www.fao.org/documents/card/en/c/cc0639en.

[74] World Food Programme (WFP), Food and Agriculture Organization of the United Nations (FAO), 2022: *Hunger Hotspots: FAO-WFP Early Warnings on Acute Food Insecurity – June to September 2022 Outlook*, https://docs.wfp.org/api/documents/WFP-0000139904/download/.

[75] The Integrated Food Security Phase Classification (IPC) is a common global scale for classifying the severity and magnitude of food insecurity and malnutrition. For Acute Food Insecurity, the system has five levels: (1) Minimal/None; (2) Stressed; (3) Crisis; (4) Emergency; (5) Catastrophe/Famine. There are similar scales for Chronic Food Insecurity and Acute Malnutrition.

[76] Hendriks, S. L.; Benton, T.; de la Mata, G. C. et al. Global Environmental Climate Change, Covid-19, and Conflict Threaten Food Security and Nutrition. *British Medical Journal* **2022**, *378*, e071534. http://dx.doi.org/10.1136/bmj-2022-071534.

[77] https://reliefweb.int/report/pakistan/ndma-monsoon-2022-daily-situation-report-no-141-dated-1st-nov-2022

[78] https://reliefweb.int/report/pakistan/wfp-pakistan-situation-report-19-september-2022

[79] World Food Programme (WFP), Food and Agriculture Organization of the United Nations (FAO), 2022: *Hunger Hotspots:* FAO-WFP *Early Warnings on Acute Food Insecurity – October 2022 to January 2023 Outlook*, https://www.wfp.org/publications/hunger-hotspots-fao-wfp-early-warnings-acute-food-insecurity-october-2022-january-2023.

[80] https://thedocs.worldbank.org/en/doc/40ebbf38f5a6b68bfc11e5273e1405d4-0090012022/related/Food-Security-Update-LXX-September-29-2022.pdf

[81] Barlow, M.; Cullen, H.; Lyon, B. Drought in Central and Southwest Asia: La Niña, the Warm Pool, and Indian Ocean Precipitation. *Journal of Climate* **2002**, 15 (7), 697–700. https://doi.org/10.1175/1520-0442(2002)015%3C0697:DICASA%3E2.0.CO;2.

[82] World Food Programme (WFP), Food and Agriculture Organization of the United Nations (FAO), 2022: *Hunger Hotspots:* FAO-WFP Early W*arnings on Acute Food Insecurity – October 2022 to January 2023 Outlook*, https://www.wfp.org/publications/hunger-hotspots-fao-wfp-early-warnings-acute-food-insecurity-october-2022-january-2023.

season from November onwards also had below-average rainfall which, combined with high costs of agricultural inputs and limited access to irrigation water, resulted in a below-average cereal harvest in 2022.[83]

In the Greater Horn of Africa, the rains failed for the fifth consecutive season since late 2020. Across the East Africa region, under the effects of the drought and other shocks, an estimated 22.5 to 23.4 million people in Ethiopia, Kenya and Somalia faced *Crisis* or worse levels of acute food insecurity as of January 2023.[84,85] Heavy rainfall and flooding in the Darfur region and Nile River basin of Sudan, and the Sudd Wetlands in South Sudan, have exacerbated crop damage, displacement, and conflictual and food insecurity conditions, putting over 7 million people at risk of *Crisis* or worse levels of acute food insecurity as of July 2022.[86] In South Sudan, four consecutive years of flooding, as well as macroeconomic challenges are expected to keep food insecurity at extreme levels. In 2022, the crop yield is expected to be below average due to widespread floods and prolonged dry spells.

As of June 2022, 28 million people were recorded as food insecure in Latin America and the Caribbean, and this food insecurity was exacerbated by the impact of hurricanes and storms. The agricultural sector in Honduras and Guatemala has been affected by increased international agricultural and food prices, with 4.6 million people in Guatemala and 2.6 million people in Honduras projected to face *Crisis* or worse levels of food insecurity.[87]

POPULATION DISPLACEMENT

Throughout the year, hazardous climate- and weather-related events and conditions played a significant role in driving new population displacement. Most people displaced in climate- or weather-related events remained within the territories where they resided, while in some situations people were forced to flee across international borders in search of safety and assistance. At the same time, climate- and weather-related hazards worsened and prolonged the situations of many of the 95 million people already living in displacement at the beginning of the year.[88]

The Horn of Africa faced its worst drought in 40 years, with Ethiopia, Kenya and Somalia particularly hard hit.[89] In Somalia, almost 1.2 million people[90] became internally displaced by the catastrophic impacts of drought on pastoral and farming livelihoods and hunger during the year.[91] Over 60 000 people fleeing the combined impacts of drought and conflict crossed

---

[83] https://reliefweb.int/report/syrian-arab-republic/giews-country-brief-syrian-arab-republic-11-january-2023

[84] https://www.fao.org/3/cc4326en/cc4326en.pdf

[85] https://reliefweb.int/report/ethiopia/amid-record-drought-and-food-insecurity-east-africas-protracted-humanitarian-crisis-worsens

[86] https://reliefweb.int/report/ethiopia/amid-record-drought-and-food-insecurity-east-africas-protracted-humanitarian-crisis-worsens

[87] https://reliefweb.int/report/world/latin-america-caribbean-weekly-situation-update-27-june-3-july-2022-4-july-2022

[88] https://www.unhcr.org/globaltrends.html and https://www.internal-displacement.org/global-report/grid2022/

[89] OCHA https://reliefweb.int/report/ethiopia/horn-africa-drought-regional-humanitarian-overview-call-action-published-4-july-2022, https://reliefweb.int/report/ethiopia/unhcr-drought-response-emergency-appeal-horn-africa

[90] https://unhcr.github.io/dataviz-somalia-prmn/index.html#reason=Drought%20related&month=&need=&pregion=&pdistrictmap=&cregion=&cdistrictmap=&year=2022

[91] https://www.unhcr.org/news/stories/somalis-abandon-their-homes-search-food-water-and-aid-drought-deepens

into Ethiopia and Kenya during the same period.[92] Concurrently, Somalia was hosting almost 35 000 refugees and asylum seekers in drought-affected areas, including over 2 600 new arrivals from Ethiopia,[93] and almost 3 million people were already living in conflict-induced internal displacement at the end of 2021.[94] A further 512 000 internal displacements associated with drought were recorded in Ethiopia. As a result of funding shortfalls and the global increase in food prices, more than 3.5 million refugees in the region (75% of the total refugee population) were affected by major cuts in food assistance.[95]

In the Syrian Arab Republic, severe winter storms, heavy snowfall and flooding damaged displacement sites, leading to more than 5 000 secondary displacements.[96] In July, devastating floods in Yemen aggravated the vulnerabilities and protection concerns of more than 10 000 displaced families, with their shelters, food and household items damaged.[97]

Record rainfall and the worst flooding in decades hit Pakistan in late August. Some 33 million people were affected, including about 800 000 Afghan refugees hosted in affected districts. By October, around 8 million people had been internally displaced by the floods, with some 585 000 sheltering in relief sites.[98] By the end of the year, with the onset of difficult winter conditions and flood waters yet to fully recede, an estimated 5 million people remained exposed to or living near flooded areas, including some 205 000 people still displaced in the provinces of Sindh and Balochistan.[99] People displaced by floods who live in informal camps, informal settlements or transitional shelters were particularly vulnerable to the cold weather, while many returnees and people who remained in flood affected areas were living in damaged, barely insulated houses.[100]

In Bangladesh, the monsoon season brought the worst floods in 20 years, affecting nearly 7.2 million people.[101] By June, 663 000 displacements had been recorded in Assam[102] and 481 000 in Sylhet and Mymensingh,[103] while in Cox's Bazar, heavy rains affected nearly 60 000 refugees and triggered secondary displacement.[104] Weather-related hazards also contributed to significant displacement in the Americas, predominantly in Brazil. In the first half of 2022, Brazil saw floods and storms which triggered a record 656 000 internal displacements.[105]

---

92 https://data.unhcr.org/en/documents/download/98367

93 https://data.unhcr.org/en/documents/download/98367

94 www.internal-displacement.org

95 https://reporting.unhcr.org/document/2953

96 https://story.internal-displacement.org/2022-mid-year-update/index.html

97 https://reliefweb.int/report/yemen/yemen-situation-update-humanitarian-impact-flooding-27-july-2022-enar

98 https://reliefweb.int/report/pakistan/unhcr-urgently-seeks-us66-million-communities-devastated-pakistan-floods, https://www.iom.int/sites/g/files/tmzbdl486/files/situation_reports/file/IOM%20External%20Sitrep_Pakistan%20floods_23September_Final.pdf, https://pakistan.iom.int/sites/g/files/tmzbdl1121/files/documents/IOM%20Pakistan%20-%20Flood%20Flash%20Appeal%20-%20Revised.pdf

99 https://reliefweb.int/attachments/188ac936-db00-46cf-bd95-898b9df526ea/Pakistan%20Floods%20Response%20SitRep%20No.13%20As%20of%206%20January%202023.pdf

100 https://reliefweb.int/report/pakistan/pakistan-2022-monsoon-floods-situation-report-no-13-6-january-2023

101 https://story.internal-displacement.org/2022-mid-year-update/index.html

102 https://story.internal-displacement.org/2022-mid-year-update/index.html

103 https://story.internal-displacement.org/2022-mid-year-update/index.html

104 https://www.humanitarianresponse.info/en/operations/bangladesh/document/iscg-flash-update-6-monsoon-response-25-august-2022

105 https://story.internal-displacement.org/2022-mid-year-update/index.html

Some high-impact weather events in 2022 happened consecutively, leaving little time for recovery between shocks and compounding repeated and protracted displacement. The southern Africa region was hit by a series of five cyclones over two months, leading to a surge in the need for protection and shelter. Hundreds of thousands of people were affected, including pre-existing refugees and people internally displaced. More than 190 000 people in Malawi who lost or fled their homes during Tropical Storm *Ana* in late January were still displaced in April.[106] In Mozambique, two months after *Ana*'s impacts included destruction of the homes and shelters of over 20 000 pre-existing internally displaced households,[107] Tropical Cyclone *Gombe* compounded its impacts, affecting over 736 000 people, damaging or destroying some 142 000 homes in many of the same areas, and forcing over 23 000 to take refuge in official shelters.[108] An assessment of existing shelter sites for internally displaced people in Nampula found that around 40% of the temporary shelters had been destroyed.[109] Meanwhile, displacement continued for over 129 000 people in Sofala Province who had been forced to flee by Tropical Cyclone *Idai* in 2019.[110]

CLIMATE IMPACTS ON ECOSYSTEMS AND THE ENVIRONMENT

Climate change has important consequences for ecosystems and the environment. For example, a recent assessment focusing on the unique high-elevation area around the Tibetan Plateau,[111] the so called Third Pole of the world and largest storehouse of snow and ice outside the Arctic and Antarctic, found that global warming is causing the temperate zone to expand.

PHENOLOGY

Phenology is the study[112] of recurring events in nature, such as when trees blossom or birds migrate, and how these are influenced by climate. Anthropogenic climate change has been shown to induce phenological shifts in terrestrial and aquatic ecosystems.[113] For example, flowering of cherry trees in Japan has been documented since AD 801 and has shifted to earlier dates since the late nineteenth century[114,115] due to the effects of climate change and

---

[106] https://www.unhcr.org/news/stories/urgent-help-needed-malawi-rebuild-lives-wrecked-tropical-storm-ana

[107] https://dtm.iom.int/reports/mozambique-tropical-storm-ana-flash-report-03-02-february-2022-0

[108] https://reliefweb.int/report/mozambique/mozambique-tropical-cyclone-gombe-flash-update-no6-25-march-2022

[109] https://reliefweb.int/report/mozambique/mozambique-tropical-cyclone-gombe-flash-update-no6-25-march-2022

[110] https://data.unhcr.org/en/documents/details/98415, https://dtm.iom.int/mozambique

[111] United Nations Environment Programme (UNEP), 2022: *A Scientific Assessment of the Third Pole Environment*, https://www.unep.org/resources/report/scientific-assessment-third-pole-environment.

[112] Hemming, D. L.; Abernethy, R.; Armitage, C. et al. Phenology of Terrestrial and Freshwater Primary Producers [in "State of the Climate in 2017"]. *Bulletin of the American Meteorological Society* **2018**, *99* (8), S63–S66. https://doi.org/10.1175/2018BAMSStateoftheClimate.1.

[113] United Nations Environment Programme (UNEP), 2022: *Frontiers 2022: Noise, Blazes and Mismatches*, https://www.unep.org/resources/frontiers-2022-noise-blazes-and-mismatches.

[114] Aono, Y. Cherry Blossom Phenological Data Since the Seventeenth Century for Edo (Tokyo), Japan, and Their Application to Estimation of March Temperatures. *International Journal of Biometeorology* **2015**, *59*, 427–434. https://doi.org/10.1007/s00484-014-0854-0.

[115] Primack, R. B.; Higuchi, H.; Miller-Rushing, A. J. The Impact of Climate Change on Cherry Trees and Other Species in Japan. *Biological Conservation* **2009**, *142* (9), 1943–1949. https://doi.org/10.1016/j.biocon.2009.03.016.

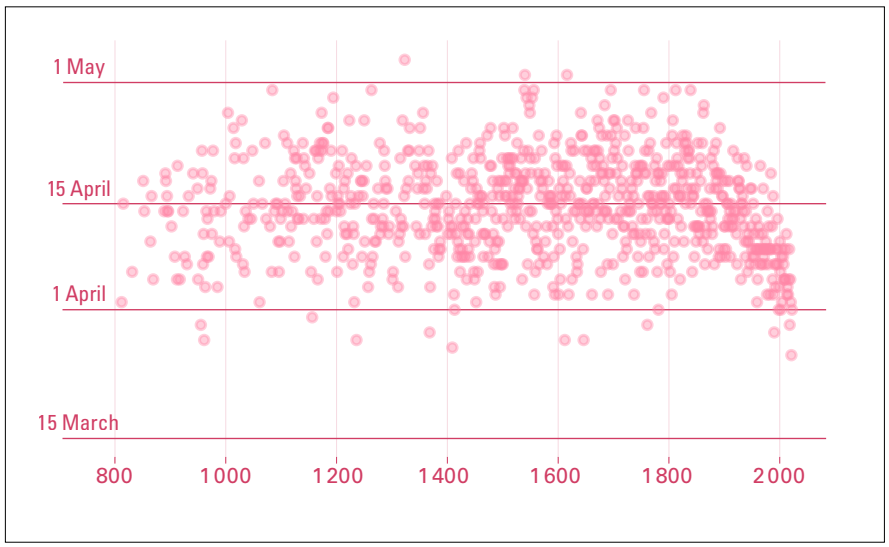

Figure 28. Full flowering date of cherry trees at Kyoto City, Japan from AD 812 to 2022.
Data from Aono, Y. Long-term Change in Climate and Floral Phenophase [in Japanese]. *Chikyu Kankyo (Global Environment)* **2012**, *17*, 21–29.

Source: John Kennedy.

urban development.[116] In 2021, the full flowering date was 26 March, the earliest recorded in over 1200 years (Figure 28). In 2022, the flowering date was 1 April.[117]

Not all species in an ecosystem respond to the same climate influences or at the same rates, which may lead to phenological mismatches that desynchronise ecological interactions and threaten ecosystem function.[118] For example, spring arrival times of 117 European migratory bird species over five decades[119] show increasing levels of phenological mismatch to other spring events, such as leaf out and insect flight, which are important for bird survival. Such mismatches are likely to have contributed to population decline in some migrant species, particularly those wintering in sub-Saharan Africa.

[116] Christidis, N.; Aono Y.; Stott P. A. Human Influence Increases the Likelihood of Extremely Early Cherry Tree Flowering in Kyoto. *Environmental Research Letters* **2022**, *17*, 054051 https://doi.org/10.1088/1748-9326/ac6bb4

[117] https://www.metoffice.gov.uk/about-us/press-office/news/weather-and-climate/2022/kyoto-cherry-blossom-dates-shifted-by-human-influence

[118] Thackeray, S.; Henrys, P.; Hemming, D. et al. Phenological Sensitivity to Climate Across Taxa and Trophic Levels. *Nature* **2016**, *535*, 241–245. https://doi.org/10.1038/nature18608.

[119] Saino, N. ; Ambrosini, R. ; Rubolini, D. et al. Climate Warming, Ecological Mismatch at Arrival and Population Decline in Migratory Birds. *Proceedings of the Royal Society B: Biological Sciences* **2011**, *278* (1707), 835–842. https://doi.org/10.1098/rspb.2010.1778.

Updating the climatological normal to 1991–2020

John Kennedy

Climatological normals are used as a benchmark against which conditions can be compared[120] (see, for example, Figure 3). They are typically based on a mean of 30 years of data. WMO guidelines recommend the use of a 30-year period ending in a '0' year, with 1991–2020 being the most recent.

In this year's report, the period 1991–2020 is used for the first time, replacing the 1981–2010 baseline. Figure 29 shows annual mean temperatures for 2022 relative to both baselines. The differences between baselines (Figure 30) are typically smaller than the variability of annual anomalies, but the same colour scale is used in both figures to aid comparison. The temperatures themselves and their rankings do not change, but the new baseline affects the anomalies, with larger areas being close to, or cooler than the new baseline. This makes patterns associated with natural variability more obvious, including La Niña and the negative phase of the Indian Ocean Dipole (see Short-term climate drivers) which were present through much of 2022.

The difference between normals for different periods can provide insight into long-term changes, though there is a 20-year overlap between the two periods. The long-term warming between 1981–2010 and 1991–2020 (Figure 30, left) was generally larger over land than the

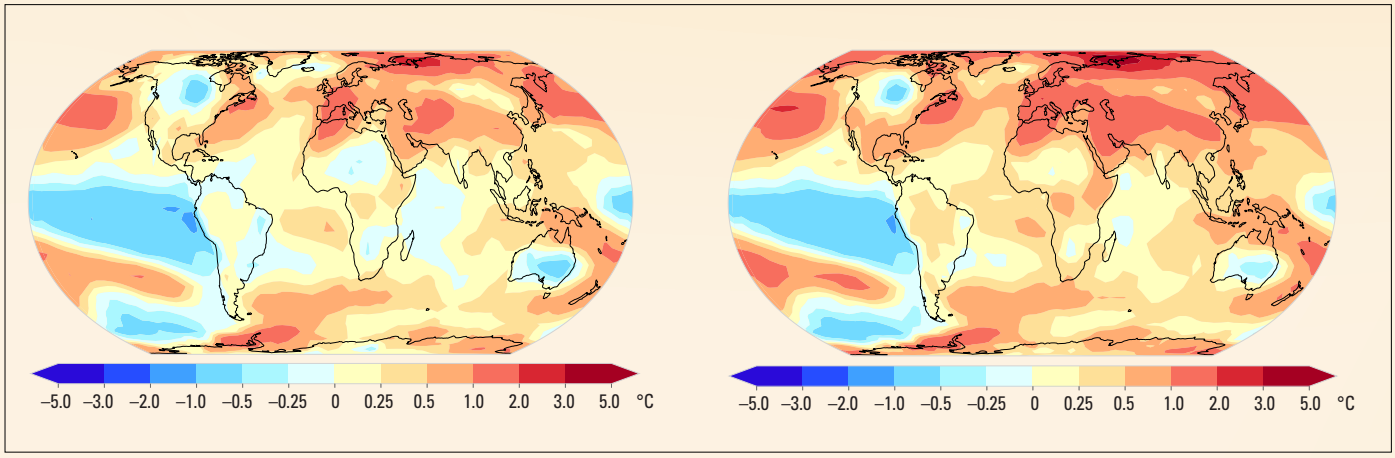

Figure 29. Annual mean temperature anomalies for 2022 relative to the (left) 1991–2020 baseline and (right) 1981–2010 baseline. Based on a median of six data sets.

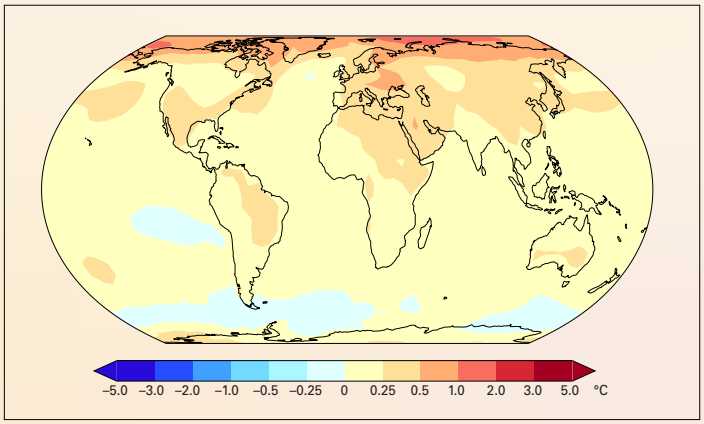

Figure 30. Difference in temperature between the 1991–2020 and 1981–2010 averages. The temperature shown is the median of six data sets.

[120] World Meteorological Organization (WMO). *The Role of Climatological Normals in a Changing Climate* (WMO/TD-No. 1377). WCDMP-No. 61. Geneva, 2007.

ocean, exceeding 0.5 °C in western Eurasia and parts of the Middle East, and was highest of all over the Arctic, where warming locally exceeded 1 °C. Limited areas of little change or weak cooling were also observed, mainly in the Southern Ocean.

Over the ocean, the areas of strongest long-term warming were in the North and South-west Pacific. There was also a limited area of cooling in the East Pacific. This pattern arises from decadal changes associated with the shift from the positive phase of the Pacific Decadal Oscillation[121] (roughly from 1980 to 2000) to the negative phase (from 2000 to present), combined with long-term warming.

The global temperature time series in the main report is shown relative to an 1850–1900 baseline. Between 1981–2010 and 1991–2020, the global mean temperature increased by 0.22 °C, from 0.77 °C to 0.99 °C above the 1850–1900 average, which is consistent with the long-term rate of temperature change of around 0.2 °C per decade.

This period 1850–1900 is used as an approximation of pre-industrial temperatures, though true pre-industrial conditions are likely to have been slightly cooler.[122] IPCC AR6 WG I estimated the difference between 1850–1900 and 1981–2010 to be 0.69 °C. To calculate anomalies relative to the earlier period, we therefore took anomalies for each data set relative to the period 1981–2010 and added 0.69 °C. The uncertainty in anomalies relative to the 1850–1900 baseline arises predominantly from the difference between the two baselines and amounts to 0.12 °C. It is not possible to calculate a reliable 1850–1900 baseline for many areas of the world because of a lack of data.

[121] Newman, M.; Alexander, M. A.; Ault, T. R. et al. The Pacific Decadal Oscillation, Revisited. *Journal of Climate* **2016**, *29* (12), 4399–4427. https://doi.org/10.1175/JCLI-D-15-0508.1.

[122] Hawkins, E.; Ortega, P.; Suckling, E. et al. Estimating Changes in Global Temperature since the Preindustrial Period. *Bulletin of the American Meteorological Society* **2017**, *98* (9), 1841–1856. https://doi.org/10.1175/BAMS-D-16-0007.1

Observational basis for climate monitoring

Climate monitoring is performed by a system of observing systems covering the atmosphere, the ocean, hydrology, the cryosphere and the biosphere. Each of these areas is monitored in different ways by a range of organizations. Cutting across all these areas, satellite observations provide major contributions to global climate monitoring.

In 1992, the Global Climate Observing System (GCOS) was established by WMO, the Intergovernmental Oceanographic Commission (IOC) of the United Nations Educational, Scientific and Cultural Organization (UNESCO), the United Nations Environment Programme (UNEP) and the International Science Council (ISC) to coordinate and facilitate the development and improvement of global climate observations. GCOS has identified a set of Essential Climate Variables (ECVs) that together provide the information necessary to understand, model and predict the trajectory of the climate as well as plan mitigation and adaptation strategies (Figure 31). The status of the observational basis for these ECVs is published in regular status reports. GCOS also identifies what is needed to improve the system in implementation reports.

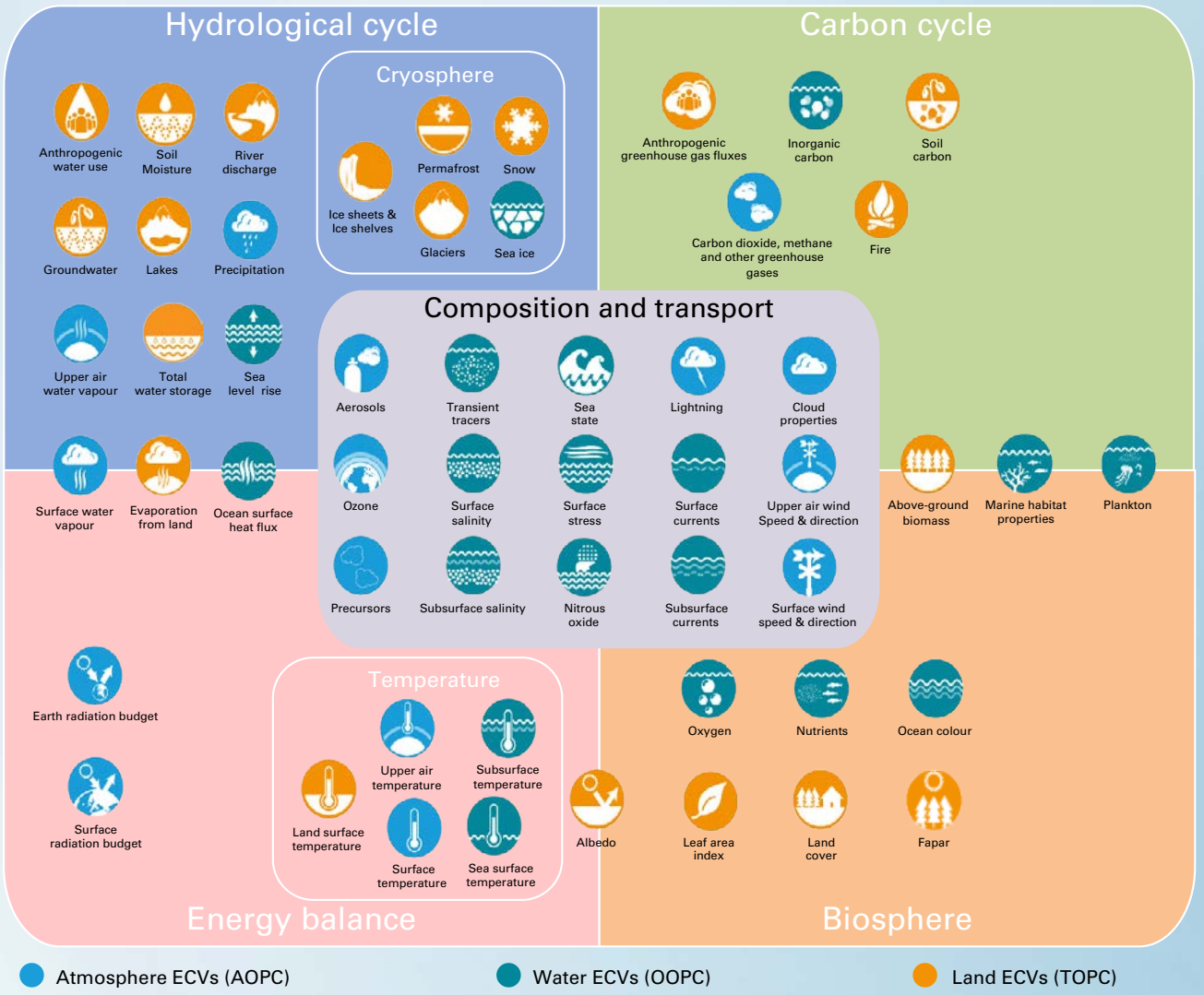

Figure 31. Essential Climate Variables (ECVs) identified by GCOS

In 2022, GCOS released its latest Implementation Plan in response to the findings of the 2021 GCOS Status Report, implications arising from the IPCC Sixth Assessment Report and recent scientific studies on the climate cycles. The publication provides recommendations for a sustained and fit for purpose Global Climate Observing System.

In addition to observations provided by the GCOS-coordinated Global Surface Network (GSN) and Global Upper-Air Network (GUAN), National Meteorological and Hydrological Services (NMHSs) of WMO Members provide a more comprehensive and widespread network of observations, acquired primarily for operational weather prediction. WMO's Global Basic Observing Network (GBON), a globally-designed network with prescribed capabilities and observing schedules and for which international data exchange is mandatory, will provide critically needed observations for numerical weather prediction and will help substantially strengthen climate reanalysis.

In order to provide the necessary financial and technical assistance for the implementation and operation of GBON in the poorest and most poorly observed areas of the globe, WMO, the United Nations Development Programme (UNDP) and UNEP have established the Systematic Observations Financing Facility (SOFF). SOFF has raised significant funds for supporting observations in least developed countries and small island developing states and commenced its implementation phase in 2023.

Complementing the observations of the physical and dynamic properties of the atmosphere, WMO's Global Atmospheric Watch (GAW) coordinates atmospheric composition measurements, ensuring that reliable and accurate data are obtained from measurements made by WMO Members, research institutions and/or agencies and other contributing networks.

Ocean observations of ocean physics, biogeochemistry, biology and ecosystems are coordinated through the Global Ocean Observing System (GOOS). The GOOS Observations Coordination Group (OCG) monitors the performance of these observations[123] and produces an annual Ocean Observing System Report Card. Ocean observations are generally made widely available to international users.

In the terrestrial domain, there is a wider group of observing networks. Hydrological observations are generally operated by NMHSs and coordinated through WMO. A number of specialized Global Terrestrial Networks (GTNs), for example, on hydrology, permafrost, glaciers, land use, and biomass, also contribute to GCOS. Data exchange agreements are generally less developed for the terrestrial networks, and many important observations are not made available to international users.

The Committee on Earth Observation Satellites/Coordination Group for Meteorological Satellites (CEOS/CGMS) Joint Working Group on Climate (WGClimate) bases the development of satellite observations for climate on the ECV requirements established by GCOS. It has produced an ECV Inventory that includes records for 766 climate data records for 33 ECVs covering 72 separate ECV products, with more planned. WGClimate is also working on actions arising from the Implementation Plan. Satellite observations have near-global coverage. Used with ground-based observations, either as complementary data sets or for validation and calibration, they form an invaluable part of the global observing system.

[123] https://www.ocean-ops.org/

Data sets and methods

GREENHOUSE GAS DATA

Estimated concentrations from 1750 are used to represent pre-industrial conditions. Calculations assume a pre-industrial mole fraction of 278.3 ppm for CO_2, 729.2 ppb for CH_4 and 270.1 ppb for N_2O.

World Data Centre for Greenhouse Gases operated by Japan Meteorological Agency https://gaw.kishou.go.jp/.

World Meteorological Organization (WMO). *WMO Greenhouse Gas Bulletin – No. 18: The State of Greenhouse Gases in the Atmosphere Based on Global Observations through 2021.* Geneva, 2022.

TEMPERATURE DATA

GLOBAL MEAN TEMPERATURE SERIES

The method for calculating global mean temperature anomalies relative to an 1850–1900 baseline is based on the assessment of long-term change and its uncertainty made by Working Group I in its contribution to the IPCC Sixth Assessment Report (IPCC AR6 WG I). The method uses shorter data sets that are routinely updated to provide an assessment of recent temperature changes.

In 2021, the IPCC AR6 WG I assessed change from 1850–1900 to other periods based on an average of four data sets – HadCRUT5, Berkeley Earth, NOAA Interim and Kadow et al. (2020) – which start in 1850. As two of the four IPCC data sets are not regularly updated, in the present report the estimate made by the IPCC for the temperature change between 1850–1900 and 1981–2010 is combined with estimated changes between 1981–2010 and the current year from six data sets to calculate anomalies for 2022 relative to 1850–1900.

There is good agreement between the six data sets on changes from 1981–2010 to the present, as this is a period with good observational coverage. The additional uncertainty from the spread of the six data sets is combined with that of the IPCC's estimate of the uncertainty in the change from 1850–1900 to 1981–2010.

Global mean temperature anomalies were calculated relative to an 1850–1900 baseline using the following steps starting from time series of global monthly mean temperatures for each data set:

1. For each data set, anomalies were calculated relative to the 1981–2010 average by subtracting the average for the period 1981–2010 for each month separately.

2. An annual average was calculated from the monthly averages.

3. The amount of 0.69 °C was added to each series, based on the estimated difference between 1850–1900 and 1981–2010, calculated using the method from IPCC AR6 WG I (see caption for Figure 1.12 in that report).

4. The mean and standard deviation of the six estimates were calculated.

5. The uncertainty in the IPCC estimate was combined with the standard deviation, assuming the two are independent and assuming the IPCC uncertainty range (0.54 °C to 0.79 °C) is representative of a 90% confidence range (1.645 standard deviations).

The number quoted in this report for 2022 (1.15 ± 0.13 °C) was calculated in this way with 1.15 °C being the mean of the six estimates.

ANNUAL TEMPERATURE MAPS

For the map of temperature anomalies for 2022, a median of six data sets was used, regridded to the spatial grid of the lowest resolution data sets (NOAAGlobalTemp and HadCRUT5), which are presented on a 5° latitude by 5° longitude grid. The median is used in preference to the mean to minimize the effect of potential outliers in individual grid cells. The half-range of the data sets provides an indication of the uncertainty. The spread between the data sets is largest at high latitudes and in Central Africa, both regions with sparse data coverage.

The following six data sets were used:

Berkeley Earth: Rohde, R. A.; Hausfather, Z. The Berkeley Earth Land/Ocean Temperature Record. *Earth System Science Data* **2020**, *12*, 3469–3479. https://doi.org/10.5194/essd-12-3469-2020.

ERA5: Hersbach, H.; Bell, B.; Berrisford, P. et al. *ERA5 Monthly Averaged Data on Single Levels from 1940 to Present*; Copernicus Climate Change Service (C3S) Climate Data Store (CDS), 2023. https://doi.org/10.24381/cds.f17050d7.

GISTEMP v4: GISTEMP Team, 2022: *GISS Surface Temperature Analysis (GISTEMP), version 4*. NASA Goddard Institute for Space Studies, https://data.giss.nasa.gov/gistemp/.
Lenssen, N.; Schmidt, G.; Hansen, J. et al. Improvements in the GISTEMP Uncertainty Model. *Journal of Geophysical Research: Atmospheres* **2019**, *124*, 6307–6326. https://doi.org/10.1029/2018JD029522.

HadCRUT.5.0.1.0: Morice, C. P.; Kennedy, J. J.; Rayner, N. A. et al. An Updated Assessment of Near-Surface Temperature Change From 1850: The HadCRUT5 Data Set. *Journal of Geophysical Research: Atmospheres* **2021**, *126*, e2019JD032361. https://doi.org/10.1029/2019JD032361.
HadCRUT.5.0.1.0 data were obtained from http://www.metoffice.gov.uk/hadobs/hadcrut5 on 1 March 2023 and are © British Crown Copyright, Met Office 2023, provided under an Open Government Licence, http://www.nationalarchives.gov.uk/doc/open-government-licence/version/3/.

JRA-55: Kobayashi, S.; Ota, Y.; Harada, Y. et al. The JRA-55 Reanalysis: General Specifications and Basic Characteristics. *Journal of the Meteorological Society of Japan*. Ser. II **2015**, *93*, 5–48. https://doi.org/10.2151/jmsj.2015-001.

NOAAGlobalTemp v5: Zhang, H.-M.; Huang, B.; Lawrimore, J. H. et al. *NOAA Global Surface Temperature Dataset (NOAAGlobalTemp), Version 5.0*. NOAA National Centers for Environmental Information. https://doi.org/10.25921/9qth-2p70.

Huang, B.; Menne, M. J.; Boyer, T. et al. Uncertainty Estimates for Sea Surface Temperature and Land Surface Air Temperature in NOAAGlobalTemp Version 5. *Journal of Climate* **2020**, *33*, 1351–1379. https://doi.org/10.1175/JCLI-D-19-0395.1.

The two additional data sets used by IPCC AR6 WG I were:

NOAA Interim: Vose, R. S.; Huang, B.; Yin, X. et al. Implementing Full Spatial Coverage in NOAA's Global Temperature Analysis. *Geophysical Research Letters* **2021**, *48*, e2020GL090873. https://doi.org/10.1029/2020GL090873.

Kadow et al.: Kadow, C.; Hall, D. M.; Ulbrich, U. Artificial Intelligence Reconstructs Missing Climate Information. *Nature Geoscience* **2020** *13*, 408–413. https://doi.org/10.1038/s41561-020-0582-5.

OCEAN HEAT CONTENT DATA

DATA USED TO 2022:

Cheng, L.; Trenberth, K. E.; Fasullo, J. et al. Improved Estimates of Ocean Heat Content from 1960 to 2015. *Science Advances* **2017**, *3*, e1601545. https://doi.org/10.1126/sciadv.1601545.

Gaillard, F.; Reynaud, T.; Thierry, V. et al. In Situ–Based Reanalysis of the Global Ocean Temperature and Salinity with ISAS: Variability of the Heat Content and Steric Height. *Journal of Climate* **2016**, *29*, 1305–1323. https://doi.org/10.1175/JCLI-D-15-0028.1.

Ishii, M.; Fukuda, Y.; Hirahara, S. et al. Accuracy of Global Upper Ocean Heat Content Estimation Expected from Present Observational Data Sets. *SOLA* **2017**, *13*, 163–167. https://doi.org/10.2151/sola.2017-030.

Kuusela, M.; Giglio, D. Global Ocean Heat Content Anomalies based on Argo Data (2.0.0). *Zenodo* **2023**. https://doi.org/10.5281/zenodo.7562281.

Levitus, S.; Antonov, J. I.; Boyer, T. P. et al. World Ocean Heat Content and Thermosteric Sea Level Change (0-2 000 m) 1955–2010. *Geophysical Research Letters* **2012**, *39*, L10603. https://doi.org/10.1029/2012GL051106.

Lyman, J. M.; Johnson, G. C. Estimating Global Ocean Heat Content Changes in the Upper 1800 m since 1950 and the Influence of Climatology Choice. *Journal of Climate* **2014**, *27*, 1945–1957. https://doi.org/10.1175/JCLI-D-12-00752.1.

von Schuckmann, K.; Le Traon, P.-Y. How Well Can We Derive Global Ocean Indicators from Argo Data? *Ocean Science* **2011**, *7*, 783–791. https://doi.org/10.5194/os-7-783-2011. Data available at: https://marine.copernicus.eu/access-data/ocean-monitoring-indicators.

ADDITIONAL DATA USED TO 2021:

Desbruyères, D. G.; Purkey, S. G.; McDonagh, E. L. et al. Deep and Abyssal Ocean Warming from 35 Years of Repeat Hydrography. *Geophysical Research Letters* **2016**, *43*, 310–356. https://doi.org/10.1002/2016GL070413.

Desbruyères, D.; McDonagh, E. L.; King, B. A. et al. Global and Full-Depth Ocean Temperature Trends during the Early Twenty-First Century from Argo and Repeat Hydrography. *Journal of Climate* **2017**, *30*, 1985–1997. https://doi.org/10.1175/JCLI-D-16-0396.1.

Good, S. A.; Martin, M. J.; Rayner, N. A. EN4: Quality Controlled Ocean Temperature and Salinity Profiles and Monthly Objective Analyses with Uncertainty Estimates. *Journal of Geophysical Research: Oceans* **2013**, *118*, 6704–6716. https://doi.org/10.1002/2013JC009067.

Hosoda, S.; Ohira, T.; Nakamura, T. A Monthly Mean Dataset of Global Oceanic Temperature and Salinity Derived from Argo Float Observations. *JAMSTEC Report of Research and Development* **2008**, *8*, 47–59. https://www.jstage.jst.go.jp/article/jamstecr/8/0/8_0_47/_article.

Kuusela M.; Stein, M. L. Locally Stationary Spatio-temporal Interpolation of Argo Profiling Float Data. *Proceedings of the Royal Society A* **2018**, *474*, 20180400. http://dx.doi.org/10.1098/rspa.2018.0400.

Li, H.; Xu, F.; Zhou, W. et al. Development of a Global Gridded Argo Data Set with Barnes Successive Corrections. *Journal of Geophysical Research: Oceans* **2017**, *122*, 866–889, https://doi.org/10.1002/2016JC012285.

Roemmich, D.; Gilson, J. The 2004–2008 Mean and Annual Cycle of Temperature, Salinity, and Steric Height in the Global Ocean from the Argo Program. *Progress in Oceanography* **2009**, *82*, 81–100. https://doi.org/10.1016/j.pocean.2009.03.004.

Roemmich, D.; Church, J.; Gilson, J. et al. Unabated Planetary Warming and its Ocean Structure Since 2006. *Nature Climate Change* **2015**, *5*, 240. https://doi.org/10.1038/nclimate2513.

ADDITIONAL DATA USED TO 2020:

Church, J. A.; White, N. J.; Konikow, L. F. et al. Revisiting the Earth's Sea-level and Energy Budgets from 1961 to 2008. *Geophysical Research Letters* **2011**, *38*. https://doi.org/10.1029/2011GL048794.

Domingues, C. M.; Church, J. A.; White, N. J. et al. Improved Estimates of Upper-ocean Warming and Multi-decadal Sea-level Rise. *Nature* **2008**, *453*, 1090–1093. https://doi.org/10.1038/nature07080.

Li, Y.; Church, J. A.; McDougall, T. J. et al. Sensitivity of Observationally Based Estimates of Ocean Heat Content and Thermal Expansion to Vertical Interpolation Schemes. *Geophysical Research Letters* **2022**, *49*, e2022G. https://doi.org/10.1029/2022GL101079.

Wijffels, S.; Roemmich, D.; Monselesan, D., et al. Ocean Temperatures Chronicle the Ongoing Warming of Earth. *Nature Climate Change* **2016**, 6, 116–118. https://doi.org/10.1038/nclimate2924.

SEA LEVEL DATA

GMSL from CNES/Aviso+ https://www.aviso.altimetry.fr/en/data/products/ocean-indicators-products/mean-sea-level/data-acces.html#c12195

Copernicus Climate Change Service (C3S), 2018: *Sea Level Daily Gridded Data from Satellite Observations for the Global Ocean from 1993 to Present*. C3S Climate Data Store (CDS), https://doi.org/10.24381/cds.4c328c78.

MARINE HEATWAVE AND MARINE COLD SPELL DATA

Marine heatwaves (MHWs) are categorized as *moderate* when the sea-surface temperature (SST) is above the 90th percentile of the climatological distribution for five days or longer; the subsequent categories are defined with respect to the difference between the SST and the climatological distribution average: *strong*, *severe* or *extreme*, if that difference is, respectively, more than two, three or four times the difference between the 90th percentile and the climatological distribution average (Hobday et al., 2018). MCS categories are analogous but counting days below the 10th percentile.

The baseline used for MHWs and MCSs is 1982–2011, which is shifted by one year from the standard normal period of 1981–2010 because the first full year of the satellite SST series on which it is based (Banzon et al. 2016) is 1982.

Hobday, A. J.; Oliver, E. C. J.; Sen Gupta, A. et al. Categorizing and Naming Marine Heatwaves. *Oceanography* **2018**, *31* (2), 1–13. https://www.jstor.org/stable/26542662.

Banzon, V.; Smith, T. M.; Chin, T. M. et al. A Long-Term Record of Blended Satellite and in Situ Sea-Surface Temperature for Climate Monitoring, Modeling and Environmental Studies. *Earth System Science Data* **2016**, *8* (1), 165–176. https://doi.org/10.5194/essd-8-165-2016.

OCEAN ACIDIFICATION DATA

Open water stations: OISO – France, Indian Ocean (data from 2010–2018); SURLATLANT – France, Atlantic Ocean (data from 2010–2018); LN6 – Iceland, Iceland Sea, North Atlantic Ocean (data from 2010–2020); K2 – Japan, North Pacific Ocean (data from 2010–2018); Chatham Island – New Zealand, South Pacific Ocean (data from 2015–2021).

Coastal water stations: Mutsu – Japan, Sekinehama Port (data from 2014–2019); Wellington – New Zealand (data from 2015–2021); L4 – United Kingdom, Western Channel Observatory (data from 2010–2019); W03 – Belgium, Scheldt Estuary (data from 2013–2020); NRSYON - Australia, Yongala National Reference Station (data from 2010–2020); REF M1V1 – Sweden, Reference Station (data from 2010–2020); Kuwait – Kuwait Bay (data from 2010–2020).

SEA ICE DATA

Data are from the EUMETSAT OSI SAF Sea Ice Index v2.1 (OSI-SAF, based on Lavergne et al., 2019 – https://osisaf-hl.met.no/v2p1-sea-ice-index) and the NSIDC v3 Sea Ice Index (Fetterer et al., 2017). Sea ice concentrations are estimated from microwave radiances measured from satellites. Extent is the area of ocean grid cells where the sea-ice concentration exceeds 15%. There are relatively large differences in the absolute extent between data sets, but they agree well on the year-to-year changes and trends. In this report, NSIDC values are reported for absolute extents, while rankings are reported for both data sets.

EUMETSAT Ocean and Sea Ice Satellite Application Facility, Sea-ice Index 1979-Onwards (v2.1, 2020), OSI-420, Data Extracted from OSI SAF FTP Server: 1979–2020, Northern and Southern Hemisphere.

Fetterer, F.; Knowles, K.; Meier, W. N. et al., 2017, updated daily. Sea Ice Index, Version 3. Boulder, Colorado, USA. National Snow and Ice Data Center (NSIDC), https://nsidc.org/data/G02135/versions/3.

Lavergne, T. Sørensen, A. M.; Kern, S. et al. Version 2 of the EUMETSAT OSI SAF and ESA CCI Sea-Ice Concentration Climate Data Records. *The Cryosphere* **2019**, *13* (1), 49–78. https://doi.org/10.5194/tc-13-49-2019.

GLACIER DATA

Glacier mass balance data for the global network of reference glaciers are available from the World Glacier Monitoring Service (WGMS), https://www.wgms.ch. Data for the 2021–2022 mass balance year are preliminary and are based on a subset of 37 (out of a total of ~42) WGMS reference glaciers.

GREENLAND AND ANTARCTIC ICE SHEET DATA

Greenland ice sheet mass balance data are reported from three sources. Modelled changes in surface mass balance and total mass balance from 1985 to 2021 are based on the average of three regional climate and mass balance models, described in Mankoff et al. (2021).

GRACE and GRACE-FO ice mass time series are calculated using spherical harmonics from JPL RL06v1, following Velicogna et al. (2020). The degree-1 geocenter terms are calculated using Sutterley and Velicogna (2019), with C2,0 and C3,0 coefficients from Loomis et al. (2019). The GRACE/GRACE-FO data are corrected for the long-term trend of glacial isostatic adjustment from the solid Earth using the regional IJ05 R2 GIA model of Ivins et al. (2013) over Antarctica and that of Simpson et al. (2009) over Greenland.

Ivins, E. R.; James, T. S.; Wahr, J. et al. Antarctic Contribution to Sea Level Rise Observed by GRACE with Improved GIA Correction. *Journal of Geophysical Research: Solid Earth* **2013**, *118*, 3126–3141. https://doi.org/10.1002/jgrb.50208.

Loomis, B. D.; Rachlin, K. E.; Luthcke, S. B. Improved Earth Oblateness Rate Reveals Increased Ice Sheet Losses and Mass-driven Sea Level Rise. *Geophysical Research Letters* **2019,** *46*, 6910–6917. https://doi.org/10.1029/2019GL082929.

Mankoff, K. D.; Fettweis, X.; Langen, P. L. et al. Greenland Ice Sheet Mass Balance from 1840 through Next Week. *Earth System Science Data* **2021**, *13* (10), 5001–5025. https://doi.org/10.5194/essd-13-5001-2021.

Simpson, M. J.; Milne, G. A.; Huybrechts, P. et al. Calibrating a Glaciological Model of the Greenland Ice Sheet from the Last Glacial Maximum to Present-day Using Field Observations of Relative Sea Level and Ice Extent. *Quaternary Science Reviews* **2009**, *28* (17), 1631–1657. https://doi.org/10.1016/j.quascirev.2009.03.004.

Sutterley, T. C.; Velicogna, I. Improved Estimates of Geocenter Variability from Time-variable Gravity and Ocean Model Outputs. *Remote Sensing* **2019**, *11* (18), 2108. https://doi.org/10.3390/rs11182108.

Velicogna I.; Mohajerani Y.; A, G. et al. Continuity of Ice Sheet Mass Loss in Greenland and Antarctica from the GRACE and GRACE Follow-On Missions, *Geophysical Research Letters* **2020,** *47*, e2020GL087291. https://doi.org/10.1029/2020GL087291.

Wiese, D. N.; Yuan, D.-N.; Boening, C. et al., 2019: JPL GRACE and GRACE-FO Mascon Ocean, Ice, and Hydrology Equivalent Water Height RL06M CRI Filtered Version 2.0, Ver. 2.0, Physical Oceanography Distributed Active Archive Center (PO.DAAC). http://dx.doi.org/10.5067/TEMSC-3MJ62.

PERMAFROST DATA

The Circumpolar Active Layer Monitoring (CALM) program of the Global Terrestrial Network for Permafrost (GTN-P) is the primary global archive of active layer thickness (ALT) data, with sites located in the Arctic, Antarctic and high mountain permafrost regions.

PRECIPITATION DATA

These Global Precipitation Climatology Centre (GPCC) data sets were used in the analysis:

- First Guess Monthly, https://doi.org/10.5676/DWD_GPCC/FG_M_100
- Monitoring Product (Version 2022), https://doi.org/10.5676/DWD_GPCC/MP_M_V2022_100
- Full Data Monthly (Version 2022), https://doi.org/10.5676/DWD_GPCC/FD_M_V2022_100
- Precipitation Climatology (Version 2022), https://doi.org/10.5676/DWD_GPCC/CLIM_M_V2022_100

In Figure 21, Iceland is shown as being drier than the long-term average. In fact, it was wetter than average in Iceland during the year (see the annual report from Iceland https://www.vedur.is/um-vi/frettir/tidarfar-arsins-2022). The discrepancy is likely due to a change in the way that real time data are processed.

List of contributors

WMO MEMBERS

Algeria, Argentina, Armenia, Australia, Bahrain, Bangladesh, Barbados, Belgium, Benin, Bosnia and Herzegovina, Brazil, British Caribbean Territories, Bulgaria, Cameroon, Canada, Cayman Islands, Chile, China, Colombia, Costa Rica, Cote d'Ivoire, Croatia, Czech Republic, Denmark, Dominica, Dominican Republic, Ecuador, Egypt, Estonia, Finland, France, Georgia, Germany, Greece, Grenada, Guatemala, Hong Kong, China; Hungary, Iceland, India, Indonesia, Islamic Republic of Iran, Iraq, Ireland, Israel, Italy, Japan, Jordan, Kazakhstan, Kenya, Latvia, Libya, Lithuania, Luxembourg, Macao, China; Madagascar, Maldives, Mali, Mauritius, Mexico, Mongolia, Montenegro, Morocco, Myanmar, Namibia, Kingdom of the Netherlands, New Zealand, North Macedonia, Norway, Pakistan, Papua New Guinea, Paraguay, Peru, Philippines, Poland, Portugal, Republic of Moldova, Russian Federation, Rwanda, Saint Kitts and Nevis, Saint Vincent and the Grenadines, Saudi Arabia, Senegal, Serbia, Seychelles, Slovakia, Slovenia, South Africa, Sri Lanka, Sweden, Switzerland, Syrian Arab Republic, Thailand, Togo, Trinidad and Tobago, Tunisia, Türkiye, Uganda, Ukraine, United Kingdom, United Republic of Tanzania, United States of America, Uruguay, Uzbekistan, Viet Nam, Zambia

INSTITUTIONS

British Antarctic Survey (BAS); Bureau of Meteorology, Australia; Carleton University, Ottawa, Canada; Carnegie Mellon University, Pittsburgh, USA; CELAD, Mercator Ocean International, Toulouse, France; Center for Ocean Mega-Science, Chinese Academy of Sciences, China; Centre for Polar Observation and Modelling (CPOM), University of Leeds, UK; Cooperative Institute for Satellite Earth Systems Studies (CICES), University of Maryland, USA; CSIRO Oceans and Atmosphere, Hobart, Tasmania, Australia; Danmarks Meteorologiske Institut (DMI); Deutscher Wetterdienst (DWD); Environment and Climate Change Canada (ECCC); ETH Zürich, Switzerland; European Centre for Medium-range Weather Forecasts (ECMWF); Geological Survey of Canada, Ottawa, Canada; GEOMAR, Kiel, Germany; George Washington University, Washington, DC, USA; Global Precipitation Climatology Centre (GPCC); ICOS Carbon Portal, Lund University, Sweden; Institut Français de Recherche pour l'Exploitation de la Mer (IFREMER), University of Brest, Centre National de la Recherche Scientifique (CNRS), Institut de Recherche pour le Développement (IRD), Laboratoire d'Océanographie Physique et Spatiale, Brest, France; Swiss Institute for Snow and Avalanche Research, SLF, Switzerland; Institute of Atmospheric Physics (IAP), Chinese Academy of Sciences, Beijing, China; Internal Displacement Monitoring Centre (IDMC); Japan Agency for Marine-Earth Science and Technology (JAMSTEC), Japan; Japan Meteorological Agency (JMA), Japan; Laboratoire d'Études en Géophysique et Océanographie Spatiales – Centre National d'Études Spatiales (LEGOS CNES), France; Magellium, France; Masaryk University, Brno, Czech Republic; Mercator Ocean International, Toulouse, France; Met Office, UK; National Oceanographic and Atmospheric Administration, Global Monitoring Laboratory (NOAA GML), USA; National Oceanographic and Atmospheric Administration, National Centers for Environmental Information (NOAA NCEI), USA; National Oceanographic and Atmospheric Administration, Pacific Marine Environmental Laboratory (NOAA PMEL), Seattle, USA; National Oceanographic Centre, Southampton, UK (NOC); Norwegian Meteorological Institute; Observatoire Midi-Pyrénées (OMP), France; Ocean Scope, Brest, France; Rutgers State University of New Jersey, USA; School of Earth Sciences, Yunnan University, Kunming, China; Science Systems and Applications, Inc. at NASA Goddard Space Flight Center, USA; Scripps Institution of Oceanography, University of California, San Diego, USA; Sorbonne Université, Centre National de la Recherche Scientifique (CNRS), Laboratoire d'Océanographie de Villefranche, France; Tohoku University, Japan; University of Brest, France; University of Calgary, Canada; University of California, Irvine, USA; University of Colorado, Boulder, USA; University of New South Wales, Sydney, Australia; University of Northern British Columbia, Canada; Vrije Universiteit Amsterdam, the Kingdom of the Netherlands; Woods Hole Oceanographic Institution, Massachusetts, USA; World Data Centre for Greenhouse Gases (WDCGG), JMA, Japan

UN AGENCIES

Food and Agriculture Organization of the United Nations (FAO), Intergovernmental Oceanographic Commission – United Nations Educational, Scientific and Cultural Organization (IOC-UNESCO), International Organization for Migration (IOM), United Nations Environment Programme (UNEP), United Nations High Commissioner for Refugees (UNHCR), United Nations Office for Disaster Risk Reduction (UNDRR), World Food Programme (WFP)

INDIVIDUAL CONTRIBUTORS

Signe Aaboe (Norwegian Meteorological Institute), Ahmat Younous Abdel-lathif (WFP), Jorge Alvar-Beltrán (FAO), Vicente Anzellini (IDMC), Chris Atkinson (Met Office, UK), Omar Baddour (publication coordinator, WMO), Paul M. Barker (University of New South Wales), Anne Barnoud (Magellium), Hamza Benlarabi (IOM), Jana Birner (UNHCR), Jessica Blunden (NCEI), Rogerio Bonifacio (WFP), Tim Boyer (NOAA NCEI), Anny Cazenave (LEGOS CNES and OMP), Xuan Che (UNDRR), Lijing Cheng (IAP; Center for Ocean Mega-Science), John Church (University of New South Wales), Damien Desbruyeres (IFREMER), Ed Dlugokencky (NOAA), Catia M. Domingues (NOC), Robert Dunn (Met Office, UK), Thomas Estilow (Rutgers State University of New Jersey), Arianna Gialletti (FAO), Donata Giglio (University of Colorado), John E. Gilson (Scripps Institution of Oceanography), Atsushi Goto (WMO), Yvan Gouzenes (LEGOS and OMP), Flora Gues (CELAD, Mercator Ocean International), Debbie Hemming (Met Office, UK), Loretta Hieber Girardet (UNDRR), Shigeki Hosoda (JAMSTEC), Sander Houweling (Vrije Universiteit Amsterdam), Filip Hrbacek (Masaryk University), Matthias Huss (ETH Zürich), Ketil Isaksen (Norwegian Meteorological Institute), Kirsten Isensee (IOC-UNESCO), Gregory C. Johnson (NOAA PMEL), Maarten Kappelle (UNEP), John Kennedy (lead author, WMO), Rachel Killick (Met Office, UK), Brian King (NOC), Nicolas Kolodziejczyk (IFREMER), Animesh Kumar (UNDRR), Mikael Kuusela (Carnegie Mellon University), Thomas Lavergne (Norwegian Meteorological Institute), Lancelot Leclercq (LEGOS), Yuehua Li (School of Earth Sciences), Ricardo Locarnini (NCEI), John Lyman (NOAA PMEL), Shawn Marshall (lead, Cryosphere section, ECCC and University of Calgary), Jesse Mason (WFP), Trevor McDougall (University of New South Wales), Brian Menounos (University of Northern British Columbia), Audrey Minère (Mercator Ocean International), Didier Paolo Monselesan (CSIRO Oceans and Atmosphere), Colin Morice (Met Office, UK), Eric R. Nash (Science Systems and Applications, Inc. at NASA Goddard Space Flight Center), Lev Neretin (FAO), Julien Nicolas (ECMWF), Jeannette Noetzli (Swiss Institute for Snow and Avalanche Research), Inès Otosaka (CPOM), Giancarlo Pini (WFP), Sylvain Ponserre (IDMC), Sarah Purkey (Scripps Institution of Oceanography), Claire Ransom (project facilitator, WMO), James Reagan (NCEI), David Robinson (Rutgers State University of New Jersey), Dean Roemmich (Scripps Institution of Oceanography), Kanako Sato (JAMSTEC), Katsunari Sato (JMA), Abhishek Savita (GEOMAR), Yousuke Sawa (JMA, WDCGG), Robert W. Schlegel (Sorbonne Université, CNRS, Laboratoire d'Océanographie de Villefranche), Katherina Schoo (IOC-UNESCO), Rahul Sengupta (UNDRR), Jose Álvaro Mendes Pimpao Alves Silva (WMO), Sharon Smith (Geological Survey of Canada), Martin Stendel (DMI), Peter Stott (Met Office, UK), Dmitry Streletskiy (George Washington University), Toshio Suga (Tohoku University; JAMSTEC), Tanguy Szekely (Ocean Scope), Oksana Tarasova (WMO), Blair Trewin (lead, Extreme events section, Bureau of Meteorology), John Turner (BAS), Freja Vamborg (ECMWF), Isabella Velicogna (University of California-Irvine), Alex Vermeulen (ICOS Carbon Portal), Karina von Schuckmann (lead, Ocean heat content section), Ying Wang (UNEP), Susan E. Wjiffels (CSIRO Oceans and Atmosphere; Woods Hole Oceanographic Institution), Michelle Yonetani (UNHCR), Markus Ziese (GPCC, DWD)

UN environment programme

Food and Agriculture Organization of the United Nations

UNHCR The UN Refugee Agency

IOM UN MIGRATION

UNDRR UN Office for Disaster Risk Reduction

WFP World Food Programme

United Nations Educational, Scientific and Cultural Organization

Intergovernmental Oceanographic Commission

For more information, please contact:

World Meteorological Organization

7 bis, avenue de la Paix – P.O. Box 2300 – CH 1211 Geneva 2 – Switzerland

Strategic Communications Office
Cabinet Office of the Secretary-General

Tel: +41 (0) 22 730 83 14 – Fax: +41 (0) 22 730 80 27

Email: communications@wmo.int

public.wmo.int

JN 23422